




Reciprocal space study of Heisenberg exchange interactions in ferromagnetic metals

Ilya V. Kashin ,* Arsenii Gerasimov , and Vladimir V. Mazurenko 

Theoretical Physics and Applied Mathematics Department, Ural Federal University, Mira Str. 19, 620002 Ekaterinburg, Russia



(Received 13 April 2022; revised 19 September 2022; accepted 28 September 2022; published 27 October 2022)

The modern quantum theory of magnetism in solids is getting commonly derived using Green's function formalism. The popularity draws itself from remarkable opportunities to capture the microscopic landscape of exchange interactions, starting from a tight-binding representation of the electronic structure. Indeed, the conventional method of infinitesimal spin rotations, considered in terms of local force theorem, opens vast prospects of investigations regarding the magnetic environment, as well as pairwise atomic couplings. However, this theoretical concept practically is not devoid of intrinsic inconsistencies. In particular, naturally expected correspondence between single and pairwise infinitesimal spin rotations is being numerically revealed to diverge. In this work, we elaborate on this question on the model example and canonical case of body-centered-cubic (bcc) iron bulk crystal. Our analytical derivations discovered the principal preference of onsite magnetic precursors if the compositions of individual atomic interactions are in focus. The problem of extremely slow or even absent spatial convergence while considering metallic compounds was solved by developed technique, based on reciprocal space framework. Using fundamental Fourier-transform-inspired interconnection between this technique and traditional spatial representation, we shed light on symmetry breaking in bcc Fe on the level of orbitally decomposed total exchange surrounding.

DOI: [10.1103/PhysRevB.106.134434](https://doi.org/10.1103/PhysRevB.106.134434)

I. INTRODUCTION

The interest of the world's physical community in the field of magnetic phenomena is gradually, but surely, shifting towards the microscopic language of description. It appears well reasoned in the context of modern technological trends towards miniaturization and energy saving, where searching of real substitution for traditional electronic semiconductor components becomes a task to be treated now. Indeed, well-known Moore's law [1,2], being empirically associated with retention of the growth rates of computing devices' productivity, completely loses its relevance. Thus, further progress in computing power demands a fundamentally new quantum vision of unit components, their interconnection, and functionality.

The quantum consideration allows one to employ any refined microelements of matter or their individual degrees of freedom as the prime driver of technologically useful effects. The atomic option immediately actualizes the formalism of spin models, designed to capture magnetic properties on the level of distinguished regular particles. The conventional object to be studied is known to be an insulator: its magnetic atomic interplay could be well described by relatively short-ranged couplings [3–8], which one could exhaustively take into account in the frame of a technically implementable numerical scheme. It results in a wide range of magnetic phenomena [9–12], described on the basis of individual atoms and molecular orbitals.

Along with the methodological task to make the spin model physically relevant and numerically solvable, its adjustment to the real material is well known to be a strictly nonstraightforward procedure. Providing that investigation was started from the first-principles calculation of electronic structure [13], the typical scheme is to construct a minimal model of magnetoactive electron shell by projecting onto Wannier functions [14].

Thus, a formulated tight-binding Hamiltonian allows one to represent the problem in the framework of Green's functions. Liechtenstein, Katsnelson, and coauthors in their pioneer works [15–19] demonstrated that application of local force theorem [20,21] to the case of infinitesimal spin rotations remarkably allows one to estimate the magnetic environment of a single atom \mathcal{J}_i , as well as particular pairwise exchange interaction J_{ij} , directly on the base of onsite and intersite Green's functions.

In this disposition, the relationship between these two approaches seems trivial:

$$\mathcal{J}_i = \sum_{j \neq i} J_{ij}. \quad (1)$$

However, numerical calculations of real insulators, conducting systems, and model crystals [22–26] keep being performed by both schemes. The preference is commonly reasoned by the focus of the study: description of individual J_{ij} favors the direct compositions, while total exchange consideration is to be estimated in its entirety. From our point of view, the question of their actual correspondence requires a detailed examination and thus manifests the main aim of this work.

*i.v.kashin@urfu.ru

Using the apparatus of onsite and intersite Green's functions to estimate exchange interactions in simple model crystals, we were able to show analytically that if one sets the electron hopping integrals spin polarized, it inevitably causes the breaking of Eq. (1) with nonlinear residuality. Consequently, the application of models with strictly onsite sources of magnetism (the Hartree-Fock method [27–30] and the dynamic mean-field theory [31–34]) for the study of conducting materials appear more accurate when spatially wide compositions of individual pairwise exchange interactions are engaged in estimation of experimentally observable characteristics.

It is important to note that such deviations are often associated with the presence of conduction electrons, which make the exchange interaction between atoms significant even at hundreds of angstroms. Indeed, the characteristic sinusoidal behavior of J_{ij} with increasing distance indicates the presence of the Ruderman-Kittel-Kasuya-Yosida (RKKY) mechanism [24,35–37]. From a theoretical point of view, this first of all means either very slow or totally absent convergence of spatial sums of pairwise exchange interactions $\sum_{j \neq i} J_{ij}$. In order to circumvent this problem, researchers often have to resort to artificial damping numerical tricks that ensure the convergence of such sums [38]. In this case, of course, additional methodological difficulties arise in the physical validation of obtained estimates.

In this regard, we develop an analytical technique, designed to find a Fourier image of pairwise exchange interactions $J(\mathbf{q})$ from corresponding Green's functions. Being derived in Ref. [22] in the frame of scattering path operator formalism, this technique was practically employed to study the spin-wave dispersion phenomena. Here we show that one can also find it remarkably useful to make a numerically stable estimation of the exchange environment in the conducting systems. Along with physical equality to J_{ij} landscape, it is particularly demonstrated that this technique could accurately produce the expected value for $\sum_{j \neq i} J_{ij}$ actual convergence dynamics for model crystals and body-centered-cubic (bcc) iron.

Authors of Ref. [39] used the $J(\mathbf{q})$ formalism in order to study the contribution of individual orbital couplings to particular J_{ij} . We also emphasize that the $J(\mathbf{q} = 0)$ point turned out to be the only source of the convergence expectations if one considers the orbitally decomposed exchange interactions. This feature enables us to study a problem concerning the net nonsuppression of cross-atomic t_{2g} - e_g interplay, which is anticipated from the cubic point-group symmetry in d magnetics. Employing Parseval's equality grants a remarkable possibility to practically examine its numerically inevitable residuality.

II. METHOD

The modern common practice for the reconstruction of equilibrium electronic, magnetic, and other characteristics of solids almost invariably includes the first-principles modeling of the electronic structure [13,40–42] as a primary stage. Further, the obtained numerical results are used to construct the so-called minimal model, the part of the system energy spectrum, which is decisive for the appearance of the properties in focus. For these purposes, the most popular approach

is to utilize a basis of maximally localized Wannier functions [14,43,44].

As a result, the minimal model is established by its Hamiltonian. The most convenient frame is known to be the tight-binding approximation [7]

$$\hat{H} = \sum_{i \neq j} \sum_{\alpha\beta} \sum_{\sigma} t_{i(\alpha)j(\beta)}^{\sigma} \hat{c}_{i(\alpha)\sigma}^{\dagger} \hat{c}_{j(\beta)\sigma} + \sum_i \sum_{\alpha} \sum_{\sigma} \varepsilon_{i(\alpha)}^{\sigma} \hat{c}_{i(\alpha)\sigma}^{\dagger} \hat{c}_{i(\alpha)\sigma}, \quad (2)$$

where $\hat{c}_{i(\alpha)\sigma}^{\dagger}$ is the creation operator of the electron with the spin σ on the orbital α of the atom i ; $\hat{c}_{j(\beta)\sigma}$ is annihilation operator of the electron with the spin σ on the orbital β of the atom j ; $t_{i(\alpha)j(\beta)}^{\sigma}$ is the corresponding hopping integral; and $\varepsilon_{i(\alpha)}^{\sigma}$ is the onsite electron energy.

This Hamiltonian can be written as a matrix function. If we express how atom i of the unit cell with translation $\mathbf{T} = 0$ interacts with the atom j of the unit cell with translation \mathbf{T} , we write

$$[H^{\sigma}(\mathbf{T})]_{ij} = t_{ij}^{\sigma} + \varepsilon_i^{\sigma} \delta_{ij} \delta_{\mathbf{T}0}, \quad (3)$$

where t_{ij}^{σ} and ε_i^{σ} are matrices, capturing the orbital structure, and δ is the Kronecker delta. Square brackets reflect the important fact that in practical calculations the Hamiltonian matrix describes the physics of the whole unit cell. Hence, the interatomic level is included as the corresponding matrix sectors ij .

Thus, Hamiltonian (3) in the reciprocal space reads as

$$H^{\sigma}(\mathbf{k}) = \sum_{\mathbf{T}} H^{\sigma}(\mathbf{T}) \cdot \exp(i\mathbf{k}\mathbf{T}). \quad (4)$$

It allows one to construct \mathbf{k} -dependent Green's function

$$G^{\sigma}(E, \mathbf{k}) = \{E - H^{\sigma}(\mathbf{k})\}^{-1}, \quad (5)$$

where E is the spectrum sweep energy in the diagonal matrix form. Then we assemble its onsite and intersite versions:

$$G_{ii}^{\sigma} = \frac{1}{N_{\mathbf{k}}} \sum_{\mathbf{k}} [G^{\sigma}(E, \mathbf{k})]_{ii}, \quad (6)$$

$$G_{ij}^{\sigma} = \frac{1}{N_{\mathbf{k}}} \sum_{\mathbf{k}} [G^{\sigma}(E, \mathbf{k})]_{ij} \cdot \exp(-i\mathbf{k}\mathbf{T}_{ij}), \quad (7)$$

where \mathbf{T}_{ij} is the translation vector connecting the cells of the i and j atoms, $N_{\mathbf{k}}$ is the number of Monkhorst-Pack grid points [45], E is an argument is omitted for brevity.

A. Isotropic exchange interactions

To find the expressions for isotropic exchange interactions we represent the electronic Hamiltonian (3) on the level of effective spin model:

$$\mathcal{H} = - \sum_{ij} J_{ij} \mathbf{e}_i \cdot \mathbf{e}_j, \quad (8)$$

where \mathbf{e}_i is the unit vector of “classically” approximated spin and each couple is taken twice.

Then, implementation of local force theorem [20,21,46] allows one to consider the second energy variation, which

occurs due to infinitesimal spin rotations near collinear ferromagnetic state, in terms of onsite and intersite Green's functions (see Appendix A for details). As the result we establish the connection between parameters of the spin and electron models:

$$\sum_{j \neq i} J_{ij} = \frac{1}{4\pi} \int_{-\infty}^{E_F} \text{Im Tr}_L [\Delta_i (G_{ii}^\uparrow - G_{ii}^\downarrow)] dE - \frac{1}{8\pi} \int_{-\infty}^{E_F} \text{Im Tr}_L \left[\sum_{\sigma} \Delta_i G_{ii}^{\sigma} \Delta_i G_{ii}^{-\sigma} \right] dE, \quad (9)$$

$$J_{ij} = \frac{1}{8\pi} \int_{-\infty}^{E_F} \text{Im Tr}_L \left[\sum_{\sigma} \Delta_i G_{ij}^{\sigma} \Delta_j G_{ji}^{-\sigma} \right] dE, \quad (10)$$

where intra-atomic spin splitting Δ_i is defined by

$$\begin{aligned} \Delta_i &= [H^\uparrow(\mathbf{T} = 0)]_{ii} - [H^\downarrow(\mathbf{T} = 0)]_{ii} \\ &= \frac{1}{N_k} \sum_{\mathbf{k}} [H^\uparrow(\mathbf{k})]_{ii} - [H^\downarrow(\mathbf{k})]_{ii}. \end{aligned} \quad (11)$$

It is clearly seen that \mathcal{J}_i [Eq. (1)] could be found both by Eqs. (9) and (10), which thereafter present single and pairwise infinitesimal spin rotations, correspondingly, as the source of energy perturbations.

However, as we show below, one could expect the non-negligible discrepancy between these two approaches. The situation appears extremely serious if one deals with metallic systems since, in that case, long-range exchange interactions strongly hamper the convergence of the real-space J_{ij} composition. For instance, authors of Ref. [38] had to take into account more than 45 coordination spheres (also referred as neighboring shells in the literature) to study spin-wave dispersion in bcc iron. Thus, in this work we elaborate the technique for numerical reconstruction of the extremely delocalized picture of magnetic interactions, based on reciprocal space framework.

B. $J(\mathbf{q})$

The mapping of all found J_{ij} values to the reciprocal space is a well-known tool that allows one to study the spin-wave dispersion spectra, the Dzyaloshinskii-Moriya interaction, spin-stiffness constants, and other magnetic phenomena [22,26,47–54].

The valuable option is that it provides an additional powerful indicator for the stability of the initial magnetic configuration, which is set by means of tight-binding Hamiltonian. The sign of \mathcal{J}_i reflects the type of total-energy extremum, which appears as the prime factor of the configuration to occur in the material or not. In its turn, the spin-wave dispersion spectrum, obtained for all reciprocal space vectors \mathbf{q} of the first Brillouin zone on the base of exchange interactions $J(\mathbf{q})$, could highlight the areas of the zone, which drive the configuration unstable [55]. Hence, we emphasize that reciprocal space consideration should be of a particular interest, especially for metallic systems.

Moving to \mathbf{q} space implies a redefinition of the basic structural units of the considered model. For this purpose we should introduce the sublattice formalism. Each sublattice comprises all crystal's atoms with equal local positions in

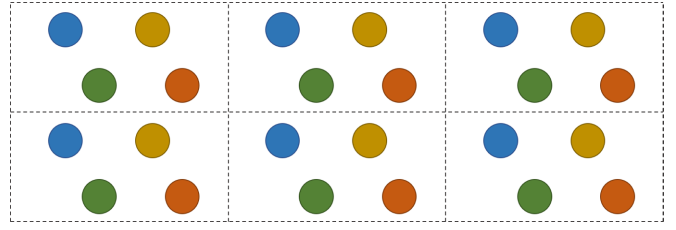


FIG. 1. Illustration of sublattice concept. Here atoms with the same local positions in the unit cells are highlighted by color. Each sublattice has the form of crystal's Bravais lattice.

the unit cells. Illustration of this concept is given in Fig. 1. Hence, notation \tilde{i} means the sublattice, formed by particular atom i and other atoms, global positions of which differ from i 's, position only by lattice translation. Thus, the elements of $[J(\mathbf{q})]_{\tilde{i}\tilde{j}}$ matrix acquire the meaning of the sublattices' interaction intensity:

$$[J(\mathbf{q})]_{\tilde{i}\tilde{j}} = \sum_{T_{ij}} J_{ij} \exp(i\mathbf{q}\mathbf{T}_{ij}). \quad (12)$$

However, due to the fact that finding all J_{ij} 's, required to compose the stable magnetic picture in metals, could be assumed intractable, a new expression is required to reconstruct $J(\mathbf{q})$ directly from the electron Green's functions.

By substituting Eq. (10) into (12), we derive

$$\begin{aligned} [J(\mathbf{q})]_{\tilde{i}\tilde{j}} &= \frac{1}{8\pi} \int_{-\infty}^{E_F} \text{Im Tr}_L \left(\sum_{\sigma} \sum_{\mathbf{k}\mathbf{k}'} \mathcal{A}_{ij}^{\sigma}(\mathbf{k}) \cdot \mathcal{A}_{ji}^{-\sigma}(\mathbf{k}') \right. \\ &\quad \left. \times \mathcal{B}_{ij}(\mathbf{k}' - \mathbf{k} + \mathbf{q}) \right) dE, \end{aligned} \quad (13)$$

where

$$\mathcal{A}_{ij}^{\sigma}(\mathbf{k}) = \frac{1}{N_k} \Delta_i [\mathcal{G}^{\sigma}(E, \mathbf{k})]_{ij}, \quad (14)$$

$$\mathcal{B}_{ij}(\mathbf{k}' - \mathbf{k} + \mathbf{q}) = \sum_{T_{ij}} \exp(i\{\mathbf{k}' - \mathbf{k} + \mathbf{q}\}\mathbf{T}_{ij}). \quad (15)$$

Taking into account that $\mathcal{B}_{ij}(\mathbf{k}' - \mathbf{k} + \mathbf{q}) = N_k \cdot \delta(\mathbf{k}' - \mathbf{k} + \mathbf{q})$, we can state the final expression:

$$[J(\mathbf{q})]_{\tilde{i}\tilde{j}} = \frac{N_k}{8\pi} \int_{-\infty}^{E_F} \text{Im Tr}_L \left(\sum_{\sigma} \sum_{\mathbf{k}} \mathcal{A}_{ij}^{\sigma}(\mathbf{k} + \mathbf{q}) \cdot \mathcal{A}_{ji}^{-\sigma}(\mathbf{k}) \right) dE. \quad (16)$$

The basic feature of this result is that derivation was performed in the framework of the pairwise infinitesimal spin-rotation technique. In this context we highlight the remarkable usefulness of $[J(\mathbf{q} = 0)]_{\tilde{i}\tilde{j}}$. Indeed, Eq. (12) in this case illustrates the straightforward possibility to reproduce \mathcal{J}_i as

$$\mathcal{J}_i = \sum_{\tilde{j}} [J(\mathbf{q} = 0)]_{\tilde{i}\tilde{j}} - \frac{1}{N_q} \sum_{\mathbf{q}} \sum_{\tilde{j}} [J(\mathbf{q})]_{\tilde{i}\tilde{j}}. \quad (17)$$

It is extremely important to note that the Fourier-transform-driven relation between J_{ij} and $[J(\mathbf{q})]_{\tilde{i}\tilde{j}}$ demands us to

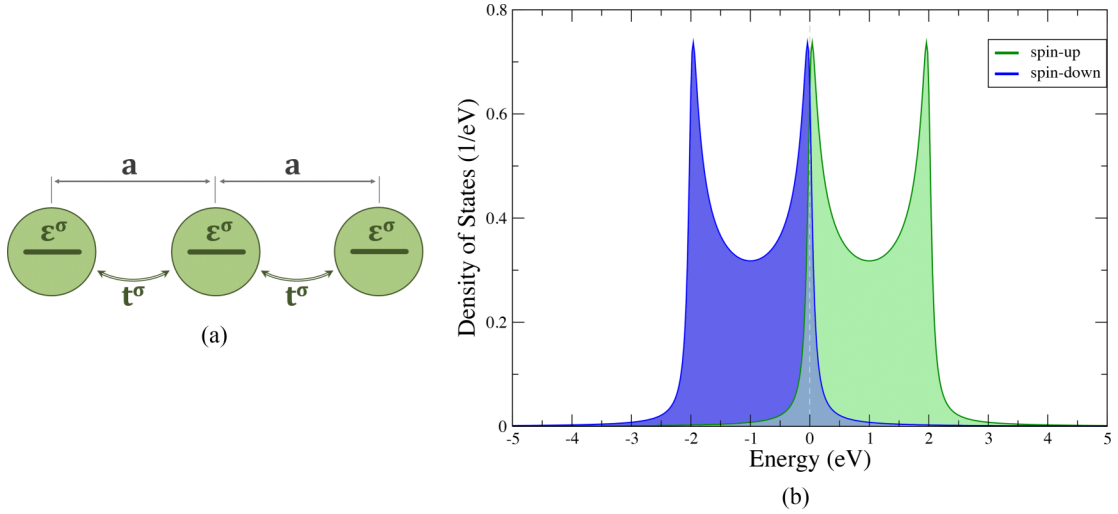


FIG. 2. (a) Schematic representation of the toy model. (b) Toy-model densities of states presented for both spin channels separately. Fermi level is set at zero.

formally define onsite parameter J_{ii} :

$$J_{ii} = \frac{1}{N_q} \sum_{\mathbf{q}} \sum_{\tilde{j}} [J(\mathbf{q})]_{i\tilde{j}}. \quad (18)$$

The valuable option is that J_{ii} could be equally calculated by Eq. (10). It reveals the lowest cost scheme of \mathcal{F}_i estimation, based only on two characteristics, being free of real spatial convergence problem and \mathbf{q} -grid density factor.

Thus, this theoretical approach actualizes itself in prospects of making a direct comparison between single and pairwise infinitesimal spin-rotation techniques on the level of representative scalars. If we denote the first term of Eq. (9) as

$$\mathcal{F}_i = \frac{1}{4\pi} \int_{-\infty}^{E_F} \text{Im Tr}_L[\Delta_i(G_{ii}^\uparrow - G_{ii}^\downarrow)] dE, \quad (19)$$

the perfect correspondence of the techniques appeared to satisfy the equation

$$\mathcal{F}_i = \sum_{\tilde{j}} [J(\mathbf{q} = 0)]_{i\tilde{j}}. \quad (20)$$

For metallic systems, this way manifests itself as the only one available, owing to the $\sum_{j \neq i} J_{ij}$ convergence problem.

We also note the self-sufficiency of reciprocal space consideration. In addition to well-known application, intended to reconstruct the spin-wave dispersion spectra [47,55–60], it is worthy to state the natural ability to find any J_{ij} by inverse Fourier transform of $J(\mathbf{q})$, calculated on some \mathbf{q} grid:

$$J(\mathbf{T}_{ij}) = \frac{1}{N_q} \sum_{\mathbf{q}} [J(\mathbf{q})]_{i\tilde{j}} \cdot \exp(-i\mathbf{q}\mathbf{T}_{ij}), \quad (21)$$

where $J(\mathbf{T}_{ij})$ is the exchange interaction matrix for the corresponding pair of crystal unit cells. Important to add that in this expression \mathbf{k} grid and \mathbf{q} grid have absolutely no constraints of being equal to each other. Further, we will practically elaborate on this question.

III. EXCHANGE SURROUNDING PROBLEM

Let us recall that in numerical calculations there is a problem of inconsistency between approaches based on a single and paired infinitesimal spin rotation. In the context of our study it could be demonstrated by independent calculation of \mathcal{F}_i using Eq. (19) and $\sum_{\tilde{j}} [J(\mathbf{q} = 0)]_{i\tilde{j}}$ using Eq. (16). Thus, obtained divergence could be readily enumerated as the residuality of Eq. (20):

$$\mathcal{D}_i = \sum_{\tilde{j}} [J(\mathbf{q} = 0)]_{i\tilde{j}} - \mathcal{F}_i. \quad (22)$$

A. Toy model

As the simplest theoretical object, we consider a *toy model* of one-dimensional extended chain of identical single-orbital atoms. This type of model could be applied to reconstruct the gapped state of real materials if the basic structure appears highly entangled [61]. It is assumed to have a period of a and one atom per unit cell. The atom in the “central” cell ($T = 0$) is denoted by i , while all other atoms are indexed by j and form the exchange surrounding of i atom [Fig. 2(a)]. We express the Hamiltonian of such a crystal as a combination of onsite energy $H^\sigma(T = 0) = \varepsilon^\sigma$ and the nearest-neighbor hoppings $H^\sigma(T = \pm a) = t^\sigma$.

For the numerical investigation we set the parameters as follows: $a = 1 \text{ \AA}$, $\varepsilon^\uparrow = -1 \text{ eV}$, $\varepsilon^\downarrow = 1 \text{ eV}$, $E_F = 0 \text{ eV}$. At the first step we assume $t^\uparrow = t^\downarrow = -0.5 \text{ eV}$. This configuration corresponds to the simplest case of spin-polarized electron structure, where two spin subsystems differ only by a simple shift along the energy axis. Figure 2(b) demonstrates that the model is designed to artificiality enhance the system’s metallicity by boosting the density of states (DOS) near the Fermi level.

It is important to note that the ground state of such system is known to be antiferromagnetic. Despite our approach being designed to provide the information about stability of the crystal in its tight-binding representation (collinear spin ordering), we assume our toy model relevant for fundamental

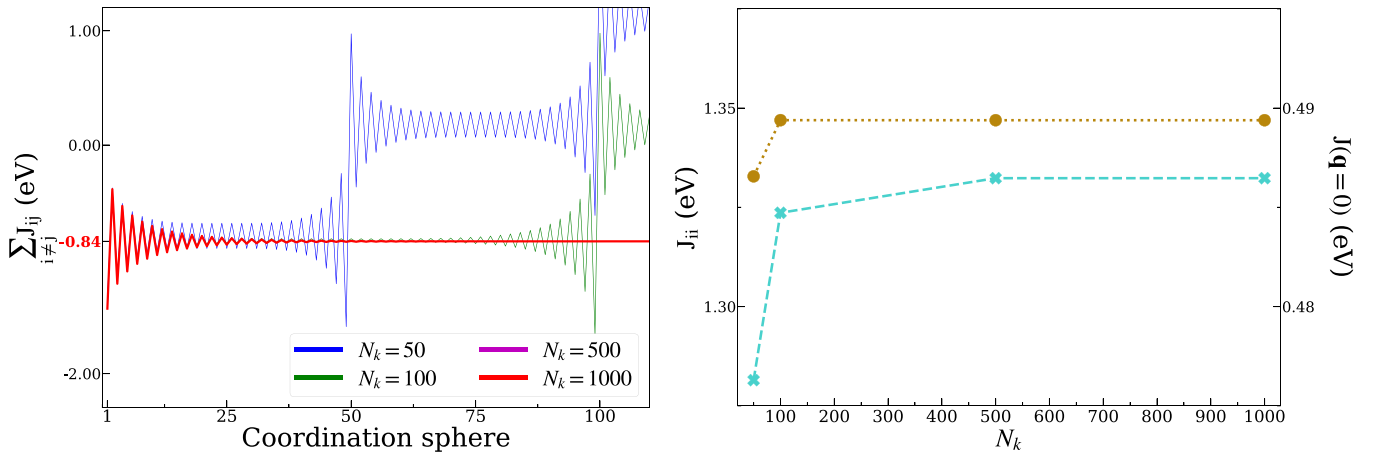


FIG. 3. (Left chart) Convergence dynamics of distance-dependent cumulative exchange interaction $\sum_{j \neq i} J_{ij}$ as more distant neighbors are taken into account. Toy-model Hamiltonian's \mathbf{k} -point mesh is $N_k \times 1 \times 1$. (Right chart) $J(\mathbf{q} = 0)$ (gold dotted) and J_{ii} (turquoise dashed) as the function of N_k .

analysis. It could be validated by the readily available option to consider two atoms in the unit cell with opposite signs of the intra-atomic spin splitting Δ , which readily states antiferromagnetism (AFM) to be energy-lowering configuration with the picture of J_{ij} kept unmodified.

The main numerical result obtained for this configuration is that $\mathcal{D} = 0$. Moreover, it appeared valid for any particular value of $t^\uparrow = t^\downarrow$ and any settings of all other parameters. Therefore, we state *the exact correspondence* of the considered approaches. Hereinafter for the crystals with one atom per unit cell for the sake of brevity we omit the single-standing index of the central atom and double indices of corresponding sublattice.

In this framework we can clearly demonstrate the advantages of $J(\mathbf{q})$ formalism developed in our study. Figure 3 (left chart) shows the dynamics of the $\sum_{j \neq i} J_{ij}$ spatial sum convergence as the contributions from more distant atoms are included. It can be seen that an increase in \mathbf{k} grid density makes the dynamics more tolerant to destabilizing high-frequency harmonics, which inevitably arise when the Hamiltonian (3) is transformed to the reciprocal space. In the case of one-dimensional \mathbf{k} grid with $N_k = 500$ and higher, the final value of the sum is expected to coincide with

$$J(\mathbf{q} = 0) - J_{ii} = \mathcal{F} - J_{ii}. \quad (23)$$

It appears instructive to add that the value of $J(\mathbf{q} = 0)$ turns out to be independent from the \mathbf{q} -grid density, in accordance with the specifics of Eq. (16).

Finding all $J(\mathbf{q})$ along some \mathbf{q} grid, we have an opportunity to estimate the J_{ij} reconstruction accuracy, according to Eq. (21). Our calculations show that if \mathbf{k} and \mathbf{q} grids are the same, any J_{ij} can be represented by *machine* precision [Fig. 4 (left chart)].

It is also extremely important to consider the case of a sparse \mathbf{k} mesh with $N_k = 50$, where the estimates of exchange interactions by Eq. (10) are confirmed unstable, as well as J_{ii} , breaking Eq. (18) by means of real- and reciprocal space configurations. Computing $J(\mathbf{q})$ on a dense \mathbf{q} grid with $N_q = 1000$, we can observe a converging dynamics of the sum of all reconstructed J_{ij} [see Fig. 4 (right chart)].

In this case, the approaching value can be estimated *exclusively* by Eq. (17), but only if J_{ii} is found as an extreme point of the inverse Fourier transform. This assessment is fully performed on the base of pairwise infinitesimal spin rotations, providing guaranteed interconnection between individual J_{ij} 's and extremely delocalized magnetic picture possessed by metals.

It is important to add that since increasing density of the \mathbf{k} grid is usually associated with a significant growth of the technical requirements for computing systems, this distinct approach has another valuable advantage as it scales the calculation time cost only, keeping random-access memory demands constant.

However, the situation with the approach's consistency changes dramatically when we consider the spin-polarized case with $t^\uparrow \neq t^\downarrow$. The complicated landscape of $\mathcal{D}(t^\uparrow, t^\downarrow)$, shown in Fig. 5, clearly demonstrates that the divergence turned out to be non-negligible and hard to predict.

We highly stress that Eq. (20) is restored exclusively in the $t^\uparrow = t^\downarrow$ regime. It makes us state the fundamental principality of the magnetism model in use, strictly onsite magnetism precursor (Hartree-Fock, LDA + DMFT), which naturally inherits this regime, or spin-polarized electron gas [local spin density approximation (LSDA)], which naturally does not.

As a matter of fact, the general relevance of both approaches is undoubtedly kept affirmed. Indeed, LSDA essentially allows to capture the spin-polarized band structure from the mean-field point of view. This point makes it reliably applicable to isotropic and homogeneous systems, or to subsystems of more complex materials, possessed by similar properties. Thus, it accordingly gives a physically valid picture of ionization energies of atoms, binding energies of solids, bulk lattice constants, anisotropic effects, etc. [59,62–65]. However, when one deals with highly inhomogeneous structures, such as strongly correlated materials [55], polarized insulators [66], or the systems with heavy fermions [67], where the electrons' distribution poses the heterogeneous nature within the unit cell, low resemblance to a noninteracting electron gas produces quantitative and qualitative discrepancies between theory and experiment. For

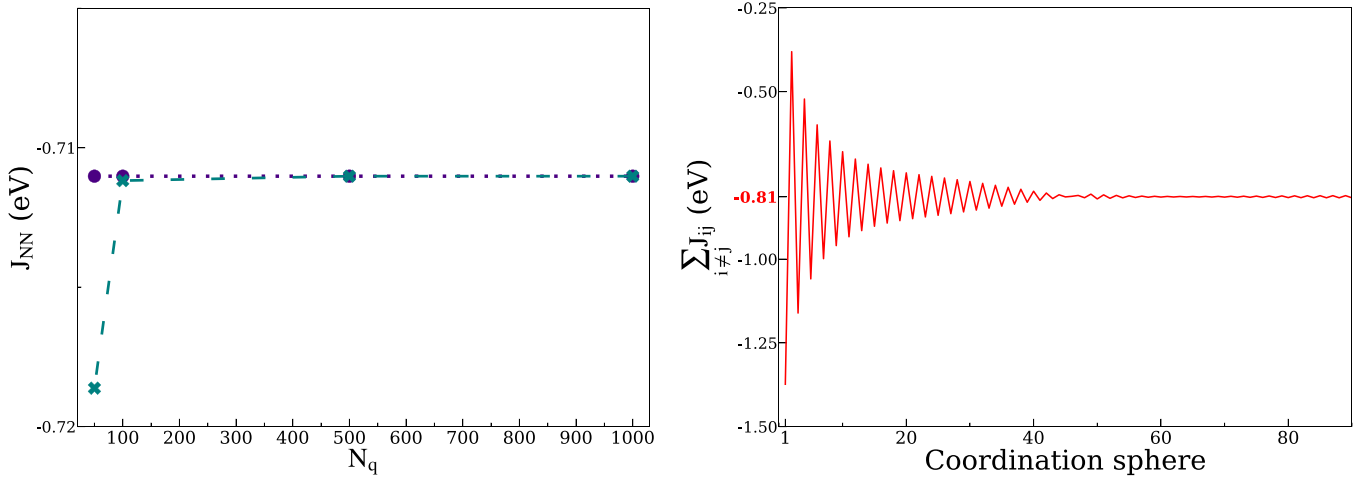


FIG. 4. (Left chart) Reconstructed using Eq. (21) (green dashed) and obtained within Eq. (10) (purple dotted) values of J_{NN} (exchange interaction between the nearest neighbors) as the function of N_q . (Right chart) Reconstructed values of J_{ij} on the sparse \mathbf{k} grid ($N_k = 50$) and dense \mathbf{q} grid ($N_q = 1000$) as the convergence dynamics of spatial sum $\sum_{j \neq i} J_{ij}$. The expected value is estimated with Eq. (17) as -0.814 eV.

instance, we can mention systematical underestimation of the band gap [62,68,69] or noncredible representation of metal-insulator transition [70–72].

On the other hand, the LDA + DMFT approach manifests itself as to rigorously capture electron-electron correlations at the focused area of the band structure. Therefore, we obtain a physically motivated access to both high- and low-energy quasiparticle excitations and, as a consequence, partly describe high-temperature properties [73–75] and paramagnetism [73,75,76]. Being usually applied to strongly correlated systems [77–79], this method turns significantly valuable, if the magnetism precursor (or, generally, the source of the investigating property) appeared isolated in the frame of well-disentangled bands. Otherwise, we face both the validation issues (double-counting problem [80]) and technical

troubles (extra large Hamiltonian to be treated). Also important to note that this approach itself is being extended methodologically, in order to capture nonlocal effects for strongly correlated electrons [81–83].

Summing up, we highlight the additional fundamental factor, which should be taken into account carefully if one intends to study collective magnetic characteristics, formed by individual or pairwise atomic contributions.

B. Analytical explanation

For a rigorous analytical substantiation of this statement, we consider a completely general case of the Hamiltonian (3), which has *spin polarized* only onsite electron energies, whereas all hoppings are kept *non-spin polarized*.

For our derivation it appears principal to keep the framework of unit-cell-sized Hamiltonian (and Green's function) matrices, implying atomic detailization incorporated. Thus, we write the Hamiltonian as a function of translation vector:

$$H^\sigma(\mathbf{T}) = t(\mathbf{T}) + \varepsilon^\sigma \delta(\mathbf{T}). \quad (24)$$

Hence, in reciprocal space we got

$$H^\sigma(\mathbf{k}) = \varepsilon^\sigma + \mathcal{H}(\mathbf{k}). \quad (25)$$

Then, if one combines the Green's functions [Eq. (5)]

$$\begin{aligned} \{\mathcal{G}^\downarrow(E, \mathbf{k})\}^{-1} - \{\mathcal{G}^\uparrow(E, \mathbf{k})\}^{-1} &= H^\uparrow(\mathbf{k}) - H^\downarrow(\mathbf{k}) \\ &= \varepsilon^\uparrow - \varepsilon^\downarrow = \Delta, \end{aligned} \quad (26)$$

the result essentially appears *independent* from \mathbf{k} .

As the next step, we rewrite Eq. (20) at the level of onsite and intersite Green's functions [16], using Eqs. (19) and (16). The same result could be obtained if we take the sum of all J_{ij} 's, calculated using Eq. (10), and assume its correspondence to Eq. (9). Here, the onsite variant is denoted by a tilde and the intersite one is given as a function of \mathbf{T} :

$$\tilde{G}^\uparrow - \tilde{G}^\downarrow = \sum_{\mathbf{T}} G^\uparrow(\mathbf{T}) \cdot \Delta \cdot G^\downarrow(-\mathbf{T}). \quad (27)$$

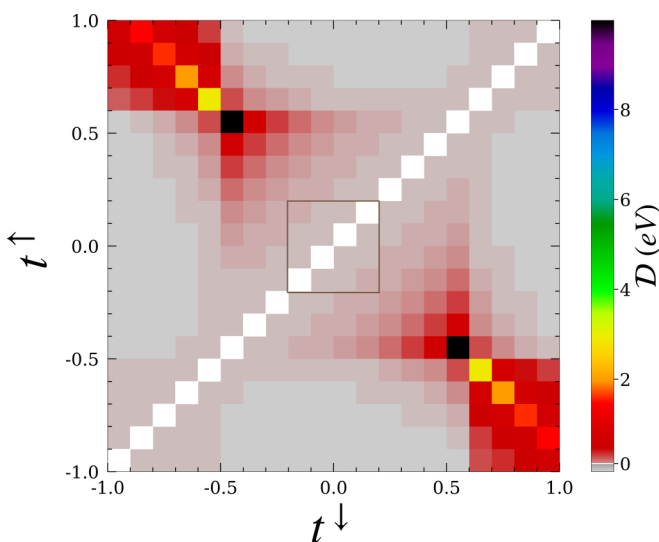


FIG. 5. Absolute value of \mathcal{D} (in eV) as a function of t^\uparrow and t^\downarrow (in eV) for the considered toy model. Gold square in the middle indicates the insulator regime $t^\sigma \ll \Delta$. Note that \mathcal{D} is exactly zero only if $t^\uparrow = t^\downarrow$ (white color).

Taking into account definitions

$$G^\uparrow(\mathbf{T}) = \frac{1}{N_{\mathbf{k}}} \sum_{\mathbf{k}} \mathcal{G}^\uparrow(E, \mathbf{k}) \cdot \exp(-i\mathbf{k}\mathbf{T}), \quad (28)$$

$$G^\downarrow(-\mathbf{T}) = \frac{1}{N_{\mathbf{k}'}} \sum_{\mathbf{k}'} \mathcal{G}^\downarrow(E, \mathbf{k}') \cdot \exp(i\mathbf{k}'\mathbf{T})$$

leads us to

$$\tilde{G}^\uparrow - \tilde{G}^\downarrow = \frac{1}{N_{\mathbf{k}}} \sum_{\mathbf{k}} \mathcal{G}^\uparrow(E, \mathbf{k}) \cdot \Delta \cdot \mathcal{G}^\downarrow(E, \mathbf{k}). \quad (29)$$

Finally, if we write Δ for any \mathbf{k} as

$$\Delta = \{\mathcal{G}^\downarrow(E, \mathbf{k})\}^{-1} - \{\mathcal{G}^\uparrow(E, \mathbf{k})\}^{-1}, \quad (30)$$

then Eq. (29) turns to identity.

Therefore, dealing with spin-polarized electron gas and then taking into account the definition of Δ [Eq. (11)], one can state \mathcal{D} [Eq. (22)] proportional to the absolute deviation of $H^\uparrow(\mathbf{k}) - H^\downarrow(\mathbf{k})$ from Δ , averaged over the first Brillouin zone. In particular, for our 1D toy model we get

$$H^\uparrow(\mathbf{k}) - H^\downarrow(\mathbf{k}) = \Delta + 2(t^\uparrow - t^\downarrow) \cos(ka) \quad (31)$$

which clearly demonstrates that $\mathcal{D} \sim t^\uparrow - t^\downarrow$.

As a consequence, we confirm a general preference for onsite-based methods of describing magnetism if we are intended to reproduce characteristics whose definitions include the spatial sums of pairwise exchange interactions.

C. bcc Fe

To elaborate the question we consider the case of real metallic material. As a bright representative in this paper let us analyze the canonical case of bcc iron. The pioneer works devoted to the first-principles study of the interatomic magnetic couplings date back to the mid 1980s [16]. However, scientific discussions do not subside until now [24,38,84–88].

In general, the reason could lie in the fact that the magnetic picture of bcc Fe cannot be exhaustively captured in frame of the Heisenberg model. Indeed, authors of the work [24] performed an orbitally resolved consideration of the nearest-neighbor Fe-Fe coupling with the initial magnetic configuration taken as one Fe moment, rotated on an arbitrary angle with respect to a collinear FM background. The t_{2g} - t_{2g} contribution appeared almost independent from this angle, whereas the t_{2g} - e_g and e_g - e_g terms were essentially modified. The former one is classified as Heisenberg interaction, driven by RKKY long-ranged mechanism, while the latter ones were described as a composition of short-ranged non-Heisenberg double-exchange and superexchange mechanisms.

Therefore, in many respects, dealing with long-ranged interplay, the controversy is supported precisely by the fact that the rate of convergence of spatial sums of exchange interactions is extremely low, which makes it difficult to make a reliable estimate of both the magnetic transition temperature and the spin-wave stiffness constants [38,88,90].

It is also noteworthy that the smallness of spin-orbital coupling in bcc Fe favors its consideration in the frame of perturbation theory. As a consequence, we do not expect J_{ij} and other isotropic characteristics being influenced by these

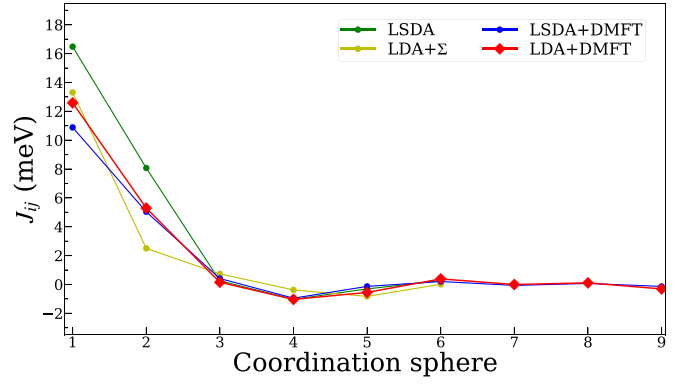


FIG. 6. Intersite exchange parameters in bcc Fe, extracted from the LDA + DMFT scheme in comparison with previous studies: green line stands for LSDA results [18], yellow for LDA + Σ [18], blue for LSDA + DMFT [89], and red line for obtained in this study LDA + DMFT.

effects on the level of Green’s functions. Whereas if one aims to study the onsite and intersite anisotropies, it appears possible by adding the corresponding terms to the spin model, which the tight-binding Hamiltonian is mapped onto.

Hence, in order to fulfill the comprehensive study of the convergence problem, we consider bcc Fe magnetism from the viewpoint of spin-polarized electron gas (LSDA) and dynamical mean-field theory (LDA + DMFT). The additional details of the calculations are given in the Appendixes B and C. Here we only mention that one atom per unit cell allows keeping the single-standing index i of the “center” atom (in the cell with $\mathbf{T} = 0$) and double index of only sublattice omitted.

In Fig. 6 one can find the comparison of the J_{ij} values, obtained in this work, with those from previous studies. At first we state a remarkable general accordance, being slightly disturbed by a factor of a particular theoretical approach in use. Apart from the first and the second nearest neighbors, which contribute dominantly to the value of the total exchange surrounding, there is a little discrepancy at the fifth coordination sphere. If the former is commonly attributed to the reason of artificial Curie temperature dependency on the particular theoretical method in use (we discuss it in Appendix D), the latter could be confidently considered nonsignificant because eight atoms on the concerning sphere are not able to influence the entire magnetic picture. Here we only mention that authors of the work [89] emphasized that such a “turbulence” at the first and the second coordination sphere is mostly driven by the qualitatively various mechanisms that t_{2g} - t_{2g} and e_g - e_g interplays generate in bcc Fe. Its competing character makes the net exchange couplings sensible to subtle aspects of theoretical approach that was employed. In Sec. IV we inspect the orbital contributions in detail.

Figure 7 (left chart) and (right chart) show the dynamics of the J_{ij} ’s convergence with the background of $\mathcal{F} - J_{ii}$ and $J(\mathbf{q} = 0) - J_{ii}$, where J_{ii} can be equivalently found both using Eqs. (10) and (18) (assuming that the \mathbf{k} and \mathbf{q} grids are the same). All results appear in a good consistence with previous studies [18,22,25,89]. As expected, the intra-atomic magnetism model, possessed by LDA + DMFT, leads the approaches based on single and pairwise spin rotations to give

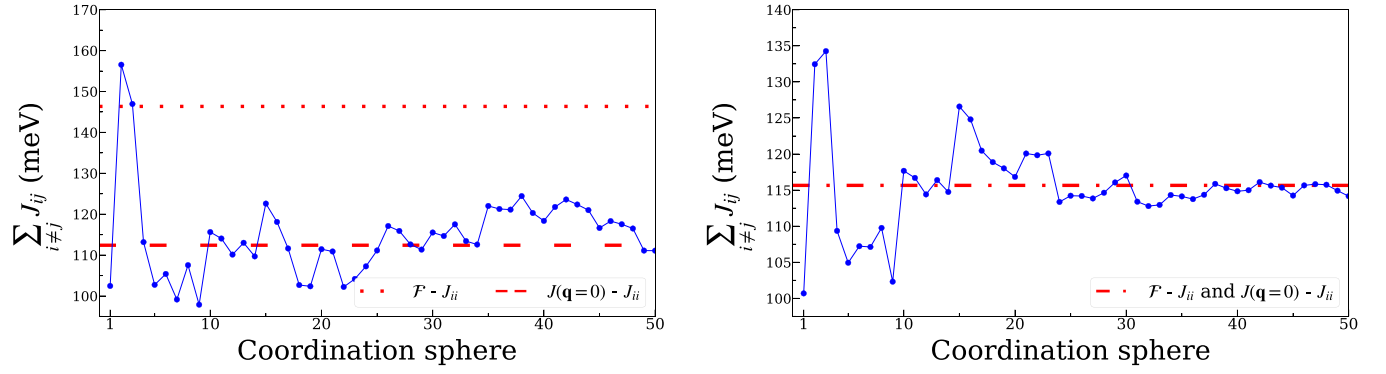


FIG. 7. (Left chart) LSDA and (right chart) LDA + DMFT originated convergence dynamics of distance-dependent cumulative exchange interaction $\sum_{j \neq i} J_{ij}$ in bcc Fe, as more distant neighbors are taken into account.

equal numerical results. The divergence is observed in the LSDA case, where the value of $J(\mathbf{q} = 0) - J_{ii}$ turns out to be reflecting actual dynamics of the convergence trend much more reliable. This confirms our basic thesis that this approach inherits all the features of the pairwise spin-rotation technique and does not lose methodological interconnection with it.

IV. ORBITAL DECOMPOSITION AND SYMMETRY PROBLEM

In addition to the considered problem, there is also a conjunction one, which the similar analysis tools appeared applicable to. Its description we should initiate by the fact that the values of exchange interactions J_{ij} [Eq. (10)] can be decomposed into the orbital components. For this, it is sufficient to turn to the mathematical property of the trace operation, taken from the product of two arbitrary $N \times N$ matrices:

$$\text{Tr}[XY] = \sum_{m=1}^N \sum_{l=1}^N X_{ml} * Y_{lm} = \sum_{m,l=1}^N Z_{ml}. \quad (32)$$

In our case, the contribution from the interaction of orbital α (atom i) with orbital β (atom j) can be found as

$$\{J_{ij}\}^{\alpha\beta} = \frac{1}{8\pi} \text{Im} \int_{-\infty}^{E_F} \{[\Delta_i G_{ij}^\uparrow]^{\alpha\beta} [\Delta_j G_{ji}^\downarrow]^{\beta\alpha} + [\Delta_i G_{ij}^\downarrow]^{\alpha\beta} [\Delta_j G_{ji}^\uparrow]^{\beta\alpha}\} dE. \quad (33)$$

Thereafter, $J_{ij} = \sum_{\alpha\beta} \{J_{ij}\}^{\alpha\beta}$. It is indicated in works [24,84,91] that thus constructed decomposition should have the symmetry properties of the crystal. In particular, when considering the d magnetism of real materials, the cubic point-group symmetry sets the expectation of the complete suppression of the contributions from the cross interaction of the t_{2g} and e_g orbitals upon the spatial summation of all J_{ij} around a particular atom i . However, actual numerical calculations of conducting materials do not justify such expectations.

Let us practically study this question in the case of bcc Fe. In Appendix D we give a full decomposition matrix $\{J_{ij}\}^{\alpha\beta}$ for one atom couple as nearest and next-nearest neighbors, being in good agreement with the work [84]. The results are additionally summarized in Table I.

In order to inspect the long-ranged interactions, in Fig. 8 we show how contributions of different symmetry orbitals to the total J_{ij} (t_{2g} - t_{2g} , e_g - e_g , and t_{2g} - e_g) individually approach the expected values, in a full accordance with the description above. It is important to note that here assessment of these expected values can be carried out only on the level of corresponding $J(\mathbf{q} = 0) - J_{ii}$ since it only inherits the orbital structure of J_{ij} . It is seen that both LSDA and LDA + DMFT do not solve the problem of nonzero $\sum_{j \neq i} \{J_{ij}\}^{t_{2g}-e_g}$, anticipated by bcc Fe symmetry.

To reveal the fundamental reasons for this discrepancy, let us pay closer attention to the fact that $J(\mathbf{q})$ and J_{ij} are related by the Fourier transform. Hence, we can write Parseval's identity [92] as

$$\sum_j |J_{ij}|^2 = \frac{1}{N_q} \sum_q |J(\mathbf{q})|^2. \quad (34)$$

By simple recombination of the terms one can obtain

$$\sum_{j \neq i} |J_{ij}|^2 - \frac{1}{N_q} \sum_{q \neq 0} |J(\mathbf{q})|^2 = \frac{1}{N_q} |J(\mathbf{q} = 0)|^2 - |J_{ii}|^2. \quad (35)$$

The symmetry of the Wannier functions of actual crystals allows us to consider the decomposition matrix $\{J_{ii}\}^{\alpha\beta}$ to be diagonal. Thereafter, in Parseval's equality, written for t_{2g} - e_g contribution, we can replace $\{J(\mathbf{q} = 0)\}^{t_{2g}-e_g}$ by $\sum_{j \neq i} \{J_{ij}\}^{t_{2g}-e_g}$ and finally obtain

$$\mathcal{P} = \sqrt{N_q \cdot \mathcal{R} - \mathcal{Q}}, \quad (36)$$

TABLE I. t_{2g} - t_{2g} , e_g - e_g , and t_{2g} - e_g contributions to J_{ij} values (in meV), obtained for the nearest (1NN) and the next-nearest (2NN) neighbors in bcc Fe.

	LSDA	LDA+DMFT	Ref. [84]
$\{J_{1NN}\}^{t_{2g}-t_{2g}}$	-10.12	-8.43	-13.95
$\{J_{1NN}\}^{e_g-e_g}$	6.66	6.49	7.67
$\{J_{1NN}\}^{t_{2g}-e_g}$	16.27	14.53	17.55
$\{J_{2NN}\}^{t_{2g}-t_{2g}}$	10.50	6.89	9.25
$\{J_{2NN}\}^{e_g-e_g}$	-1.50	-1.60	-0.76
$\{J_{2NN}\}^{t_{2g}-e_g}$	0.00	0.00	0.00

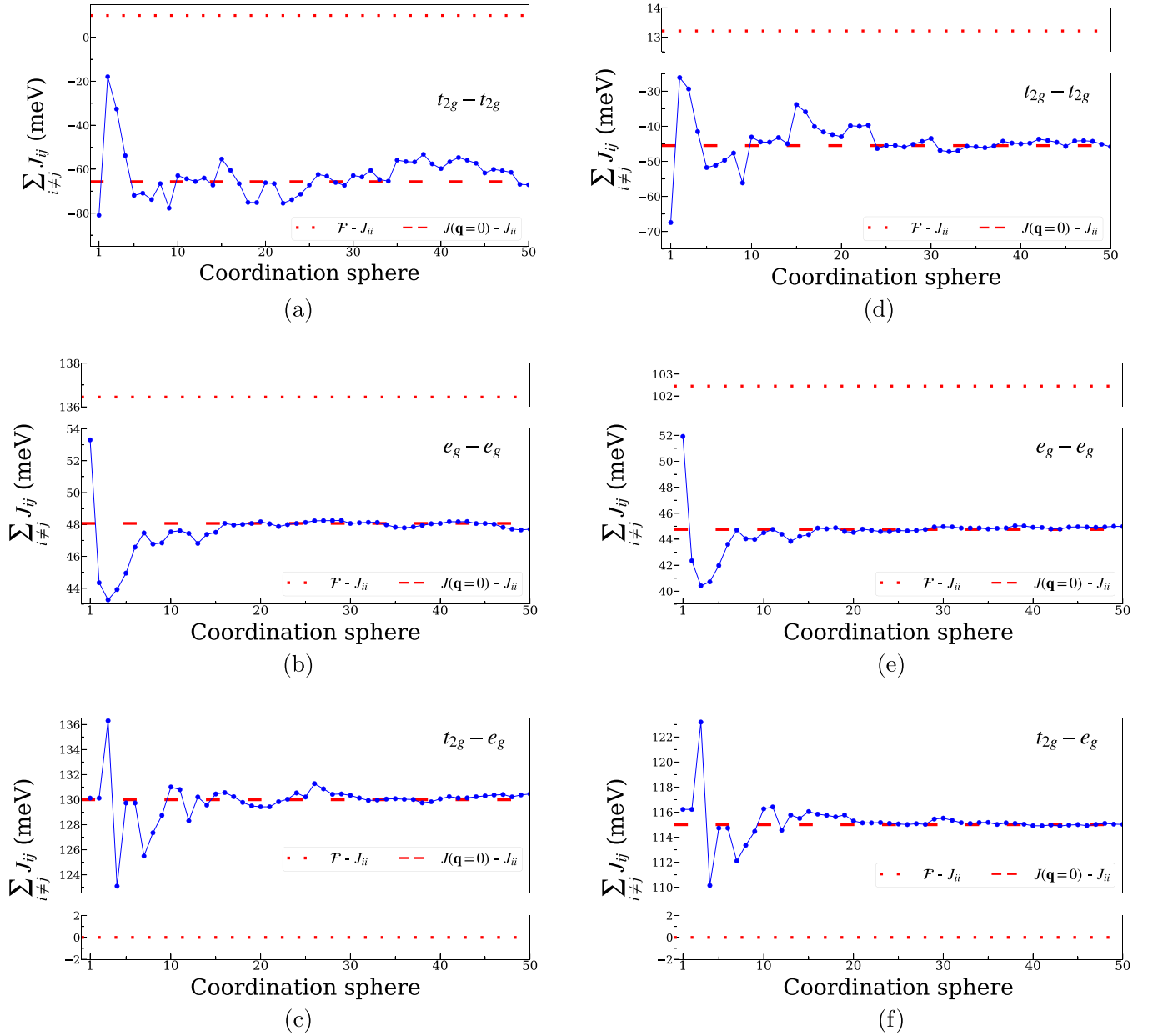


FIG. 8. LSDA originated convergence dynamics of orbital-resolved distance-dependent cumulative exchange interactions (a) $\sum_{j \neq i} \{J_{ij}\}^{t_{2g}-t_{2g}}$, (b) $\sum_{j \neq i} \{J_{ij}\}^{e_g-e_g}$, and (c) $\sum_{j \neq i} \{J_{ij}\}^{t_{2g}-e_g}$ in bcc Fe versus LDA + DMFT originated convergence dynamics of orbital-resolved distance-dependent cumulative exchange interactions (d) $\sum_{j \neq i} \{J_{ij}\}^{t_{2g}-t_{2g}}$, (e) $\sum_{j \neq i} \{J_{ij}\}^{e_g-e_g}$, and (f) $\sum_{j \neq i} \{J_{ij}\}^{t_{2g}-e_g}$ in bcc Fe, as more distant neighbors are taken into account.

where

$$\mathcal{P} = \left| \sum_{j \neq i} \{J_{ij}\}^{t_{2g}-e_g} \right|, \quad (37)$$

$$\mathcal{R} = \sum_{j \neq i} |\{J_{ij}\}^{t_{2g}-e_g}|^2, \quad (38)$$

$$\mathcal{Q} = \sum_{\mathbf{q} \neq 0} |\{J(\mathbf{q})\}^{t_{2g}-e_g}|^2. \quad (39)$$

Each of the thus introduced parts deserves specific attention. It appears that \mathcal{R} has a remarkable feature: more than 98% of the net value (obtained as sum over 50 coordination

spheres) comes from *the nearest neighbors*, while 6 coordination spheres cover 99.8% [Fig. 9 (left chart)].

Thereafter, we can confidently state \mathcal{R} as *converged constant*. In view of this fact the next step can be checking \mathcal{P} for an ability to reproduce its expected value $|\{J(\mathbf{q}=0)\}^{t_{2g}-e_g}|$ (130 meV), by separated means of \mathbf{q} grid density. Figure 9 (right chart) shows that it actually takes place if the density is $25 \times 25 \times 25$ or more. On one hand, it additionally confirms the fundamental consistency of our theoretical approach. On the other hand, it alone does not lift the veil from the problem of \mathcal{P} nonsuppression due to the crystal's symmetry.

For the latter purpose we utilize the constancy of \mathcal{R} as the ground of the following analysis. Anticipation of $\mathcal{P} = 0$

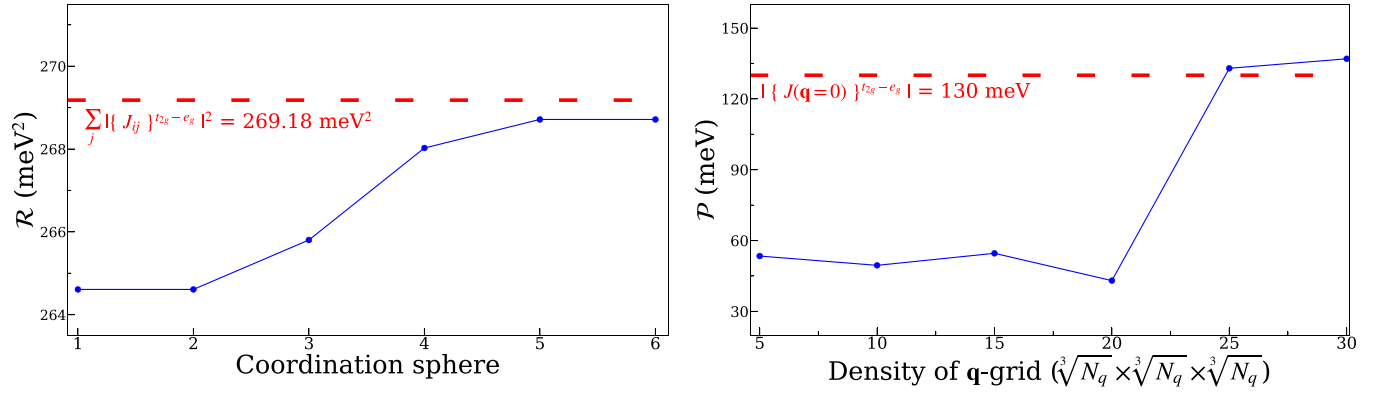


FIG. 9. (Left chart) \mathcal{R} [Eq. (38)] obtained for bcc Fe using LSDA, as more distant neighbors are taken into account. The expected value is estimated as the combination of individual pairwise contributions up to 50th coordination sphere. (Right chart) \mathcal{P} [Eq. (37)] obtained for bcc Fe using LSDA, as a function of \mathbf{q} -grid density $\sqrt[3]{N_q} \times \sqrt[3]{N_q} \times \sqrt[3]{N_q}$.

in this disposition demands \mathcal{Q} [Eq. (39)] to be *linearly* proportional to N_q . To study the actual dependency we represent \mathcal{Q} as

$$\mathcal{Q} = \text{const} \times (N_q)^\gamma, \quad (40)$$

where constant is implied to be in meV^2 . Consequently, for γ we get

$$\gamma = \frac{d\{\ln(\mathcal{Q})\}}{d\{\ln(N_q)\}}. \quad (41)$$

Results are shown in Table II. Here we highlight that divergence of γ from ideal value 1 is observed on the constant level of $\sim 0.5\%$ (excluding the topmost point). Taking to account the coverage of both areas of consistent and nonconsistent \mathcal{P} , we can conclude this divergence to be possessed by our theoretical formalism itself. Providing that $N_q \cdot \mathcal{R}$ and \mathcal{Q} are naturally large, it finally causes throttling the symmetry driver of \mathcal{P} , at least on the computationally available grids. In order to affirm this statement let us approximate numerically obtained $\ln(\mathcal{Q})[\ln(N_q)]$ curve by its perfect version with $\gamma = 1$:

$$\ln(\mathcal{Q}) \approx \ln(\mathcal{R}') + \ln(N_q). \quad (42)$$

Thus, $\mathcal{R}' = 268.27 \text{ meV}^2$ diverges from calculated \mathcal{R} by less than 1 meV^2 . It reveals the general tendency of \mathcal{P} towards suppression if we assume $N_q \rightarrow \infty$ in an extrapolating manner.

TABLE II. Estimation of γ [Eq. (41)] using finite-difference method.

\mathbf{q} grid	$\ln(N_q)$	$\ln(\mathcal{Q})$	γ
$5 \times 5 \times 5$	4.82831	10.33496	
$10 \times 10 \times 10$	6.90776	12.49399	1.03827
$15 \times 15 \times 15$	8.12415	13.71624	1.00482
$20 \times 20 \times 20$	8.98720	14.58171	1.00281
$25 \times 25 \times 25$	9.65663	15.24779	0.99499
$30 \times 30 \times 30$	10.20359	15.79638	1.00297

V. CONCLUSIONS

In this work we elaborate on the question of self-consistency and convergence, if one employs the local force theorem to study real and model conducting materials at the level of exchange landscape in the pairwise details, as well as in its entirety. It was showed analytically and numerically that the choice of magnetism's precursor has a decisive influence on the validation and accuracy of the theoretically reconstructed magnetic picture. It is important to supplement the earlier remark about the preference of using onsite sources (the Hartree-Fock method and DMFT) with a cautionary note to use *combined* approaches in a manner of LSDA + DMFT for a study of characteristics, which essentially are formed as the sum of individual atomic contributions. In addition to the naturally arising complexity due to the double-counting problem, the fundamental uncertainty of the source of magnetism will not allow one to control the consistency of infinitesimal spin-rotation-based approaches.

We were also able to shed light on the problem of symmetry breaking at the level of orbital decomposition while accumulating the spatial sums of pairwise exchange interactions in conducting systems. Consideration of the canonical bcc Fe case in the frame of suggested reciprocal space approach showed the origins of the vanishingly low rates of symmetry-reasoned suppression of contributions from the interaction of t_{2g} and e_g orbitals, leading to nonzero values of those in practical calculations.

The obtained theoretical results are believed to be of significant usefulness while elaborating on the general question of long-range magnetic ordering in real metallic compounds, which stands in veil during numerical misconceptions of the present approaches.

ACKNOWLEDGMENTS

The authors acknowledge A. Szilva, Y. Kvashnin, I. Miranda, and O. Eriksson for fruitful and inspiring discussions. The work of I.V.K. and A.G. is supported by the grant program of the President of the Russian Federation Grant No. MK-2578.2021.1.2. The work of V.V.M. is supported by the Russian Science Foundation, Grant No. 21-72-10136. The

computer simulations are performed on computational resources provided by the Uran supercomputer allocated by the IMM UB RAS.

APPENDIX A: EXCHANGE INTERACTION EXPRESSIONS

In order to estimate the picture of isotropic exchange interactions, we should perform a mapping of the original electronic model [tight-binding Hamiltonian (3) in the main text] onto the effective spin model:

$$\mathcal{H} = - \sum_{ij} J_{ij} \mathbf{e}_i \cdot \mathbf{e}_j. \quad (\text{A1})$$

For this purpose the initial configuration is assumed to be purely ferromagnetic: $\mathbf{e}_i = (0, 0, 1)$. Let us then consider an infinitesimal spin rotation on an angle $\delta\boldsymbol{\phi} = \delta\phi \cdot \mathbf{n}$, where $\mathbf{n} = (n_x, n_y, 0)$ is the axis direction. The thus caused energy perturbation one can describe by calculating the second variation of Eq. (A1):

$$\delta^2 \mathcal{H} = - \sum_{ij} J_{ij} [\delta^2 \mathbf{e}_i \cdot \mathbf{e}_j + 2 \delta \mathbf{e}_i \cdot \delta \mathbf{e}_j + \mathbf{e}_i \cdot \delta^2 \mathbf{e}_j], \quad (\text{A2})$$

where

$$\begin{aligned} \delta \mathbf{e}_i &= [\delta\boldsymbol{\phi}_i \times \mathbf{e}_i] = (\delta\phi_i^y, -\delta\phi_i^x, 0), \\ \delta^2 \mathbf{e}_i &= [\delta\boldsymbol{\phi}_i \times \delta \mathbf{e}_i] = -(0, 0, \delta^2 \phi_i^x + \delta^2 \phi_i^y). \end{aligned} \quad (\text{A3})$$

Thereby, Eq. (A2) takes the final form

$$\begin{aligned} \delta^2 \mathcal{H} &= \sum_i \left\{ \sum_j J_{ij} (\delta^2 \phi_i^x + \delta^2 \phi_i^y) \right\} \\ &+ \sum_j \left\{ \sum_i J_{ij} (\delta^2 \phi_j^x + \delta^2 \phi_j^y) \right\} \\ &+ \sum_{ij} \{-2 J_{ij} (\delta\phi_i^x \delta\phi_j^x + \delta\phi_i^y \delta\phi_j^y)\}. \end{aligned} \quad (\text{A4})$$

As the next step we should employ the local force theorem [20,21,46] to the electronic Hamiltonian. According to this theorem, the total-energy variation $\delta\mathcal{E}$, caused by small perturbation from the ground state of the system, could be represented as the sum of one-particle energy changes of the occupied states, with ground-state potential kept fixed. In terms of first-order perturbations we write for charge and spin densities [16]

$$\begin{aligned} \delta\mathcal{E} &= \int_{-\infty}^{E_F} E \delta\tilde{n}(E) dE \\ &= E_F \delta Z - \int_{-\infty}^{E_F} \delta\tilde{N}(E) dE = - \int_{-\infty}^{E_F} \delta\tilde{N}(E) dE, \end{aligned} \quad (\text{A5})$$

where $\tilde{n}(E) = d\tilde{N}(E)/dE$ is the density of electron states, $\tilde{N}(E)$ its integrated version, E_F is the Fermi energy, δZ is the change of total number of electrons, being zero if we consider magnetic excitation case.

Assuming H and G to be short spinor notations of the electronic Hamiltonian and Green's function [Eq. (5) in the

main text] for $\tilde{n}(E)$ one can write

$$\tilde{n}(E) = -\frac{1}{\pi} \text{Im Tr}_{\text{L},\sigma}[G], \quad (\text{A6})$$

which leads to the following expression for $\delta\tilde{N}(E)$:

$$\delta\tilde{N}(E) = \frac{1}{\pi} \text{Im Tr}_{\text{L},\sigma}[\delta H G], \quad (\text{A7})$$

where $\text{Tr}_{\text{L},\sigma}$ denotes the trace over orbital (L) and spin (σ) indices.

Consequently, the second variation of total energy could be expressed as

$$\delta^2 \mathcal{E} = -\frac{1}{\pi} \int_{-\infty}^{E_F} \text{Im Tr}_{\text{L},\sigma}[\delta^2 H G + \delta H G \delta H G] dE. \quad (\text{A8})$$

In order to consider the spin rotation by $\delta\boldsymbol{\phi}$ on the level of electron model, we should introduce the corresponding operator

$$\hat{U} = \exp(i \frac{1}{2} \delta\boldsymbol{\phi} \cdot \hat{\boldsymbol{\sigma}}), \quad (\text{A9})$$

where $\hat{\boldsymbol{\sigma}} = (\hat{\sigma}_x, \hat{\sigma}_y, \hat{\sigma}_z)$ are Pauli matrices. Providing that $\delta\boldsymbol{\phi}$ is small, one can perform the expansion

$$\hat{U} \approx 1 + i \frac{1}{2} \delta\boldsymbol{\phi} \cdot \hat{\boldsymbol{\sigma}} - \frac{1}{8} (\delta\boldsymbol{\phi} \cdot \hat{\boldsymbol{\sigma}})^2. \quad (\text{A10})$$

Then, being applied to the electronic Hamiltonian, this operator generates the first and the second variations for atom i as follows:

$$\delta H_{ii} = \frac{\Delta_i}{2} \left\{ i \delta\phi_i^x \begin{pmatrix} 0 & 1 \\ -1 & 0 \end{pmatrix} + \delta\phi_i^y \begin{pmatrix} 0 & 1 \\ 1 & 0 \end{pmatrix} \right\}, \quad (\text{A11})$$

$$\delta^2 H_{ii} = \frac{\Delta_i}{2} \begin{pmatrix} -1 & 0 \\ 0 & 1 \end{pmatrix} (\delta^2 \phi_i^x + \delta^2 \phi_i^y). \quad (\text{A12})$$

Thereby, the second variation of electron system reads as

$$\begin{aligned} \delta^2 \mathcal{E} &= -\frac{1}{\pi} \int_{-\infty}^{E_F} \text{Im Tr}_{\text{L}} \left\{ \frac{1}{2} \left[\sum_i \text{Tr}_{\sigma} (\delta^2 H_{ii} G_{ii}) \right] \right. \\ &+ \frac{1}{2} \left[\sum_j \text{Tr}_{\sigma} (\delta^2 H_{jj} G_{jj}) \right] \\ &+ \frac{1}{2} \left[\sum_i \text{Tr}_{\sigma} (\delta H_{ii} G_{ii} \delta H_{ii} G_{ii}) \right] \\ &+ \frac{1}{2} \left[\sum_j \text{Tr}_{\sigma} (\delta H_{jj} G_{jj} \delta H_{jj} G_{jj}) \right] \\ &\left. + \left[\sum_{ij, i \neq j} \text{Tr}_{\sigma} (\delta H_{ii} G_{ij} \delta H_{jj} G_{ji}) \right] \right\} dE, \end{aligned} \quad (\text{A13})$$

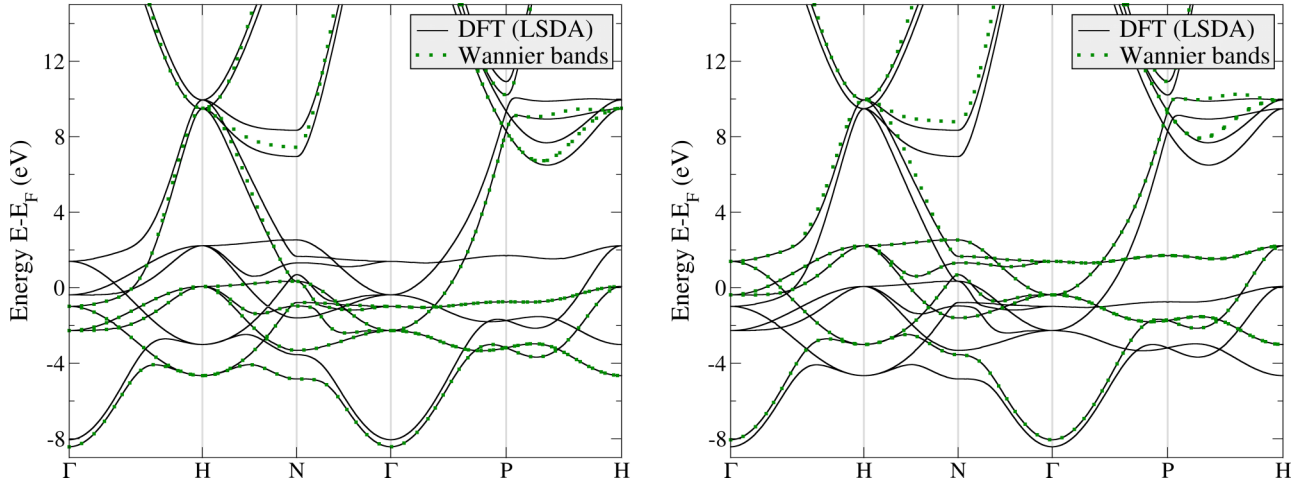


FIG. 10. Comparison of magnetic band structures of bcc iron calculated using the full-potential linearized augmented plane waves in LSDA approach (black lines) and low-energy model in Wannier functions basis of spd character (green dotted lines). (Left) Spin-down states. (Right) Spin-up states. The Fermi level corresponds to the zero energy.

where

$$\begin{aligned} & \text{Tr}_\sigma (\delta^2 H_{ii} G_{ii}) \\ &= -\frac{1}{2} \Delta_i (G_{ii}^\uparrow - G_{ii}^\downarrow) (\delta^2 \phi_i^x + \delta^2 \phi_i^y), \\ & \text{Tr}_\sigma (\delta H_{ij} G_{ij} \delta H_{jj} G_{ji}) \\ &= \frac{1}{4} \left\{ \sum_\sigma \Delta_i G_{ij}^\sigma \Delta_j G_{ji}^{-\sigma} \right\} (\delta \phi_i^x \delta \phi_j^x + \delta \phi_i^y \delta \phi_j^y), \quad (\text{A14}) \end{aligned}$$

and $-\sigma$ implies opposite spin direction to σ .

Finally, by matching Eq. (A13) with (A4), we come to the following regular expressions for particular atom i and couple ij :

$$\begin{aligned} & \delta^2 \phi_i^x + \delta^2 \phi_i^y : \\ & \sum_{j \neq i} J_{ij} = \frac{1}{4\pi} \int_{-\infty}^{E_F} \text{Im Tr}_L [\Delta_i (G_{ii}^\uparrow - G_{ii}^\downarrow)] dE \\ & \quad - \frac{1}{8\pi} \int_{-\infty}^{E_F} \text{Im Tr}_L \left[\sum_\sigma \Delta_i G_{ii}^\sigma \Delta_i G_{ii}^{-\sigma} \right] dE, \quad (\text{A15}) \end{aligned}$$

$$\begin{aligned} & \delta \phi_i^x \delta \phi_j^x + \delta \phi_i^y \delta \phi_j^y : \\ & J_{ij} = \frac{1}{8\pi} \int_{-\infty}^{E_F} \text{Im Tr}_L \left[\sum_\sigma \Delta_i G_{ij}^\sigma \Delta_j G_{ji}^{-\sigma} \right] dE. \quad (\text{A16}) \end{aligned}$$

It is worth mentioning that there are other techniques designed to make a correspondence between Heisenberg Hamiltonian and the DFT calculations by means of energy fitting [93,94] and also MFT-based one [39,54].

APPENDIX B: DFT CALCULATIONS, WANNIER FUNCTIONS, AND TIGHT-BINDING HAMILTONIANS

Electronic properties of bcc crystal structure of iron were simulated using an *ab initio* approach, where authors first performed LSDA calculations with exchange-correlation

functional in the Perdew-Wang and Ceperley-Alder form [95] as implemented in the ELK code [96,97]. The calculation parameters are as follows. We used $a_{Fe} = 2.71 \text{ \AA}$ lattice parameter and $(20 \times 20 \times 20)$ Monkhorst-Pack k -point grid for the integration in reciprocal space over the Brillouin zone.

Figure 10 shows the calculated spin-polarized electronic energy spectrum of the bcc Fe. Afterwards, the ‘‘Wannierization’’ procedure was applied to construct an effective Hamiltonian in the basis of the maximally localized Wannier functions [44] for both spin states separately, where we projected the bands on the orbitals of s , p , and d characters using a WANNIER90 code [98,99] and the ELK to WANNIER90 programming interface [75]. Calculated magnetic moment per iron atom was found to be equal to $2.20 \mu_B$, which is about experimental value [100].

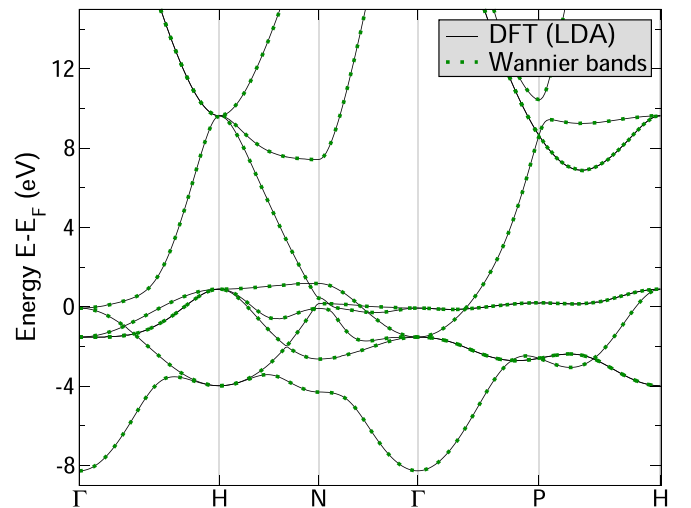


FIG. 11. Comparison of nonmagnetic band structures of bcc Fe calculated using the full-potential linearized augmented plane waves within LDA approximation (black lines) and low-energy model in Wannier functions basis of spd character (green dotted lines). The Fermi level corresponds to the zero energy.

TABLE III. Orbital-decomposed J_{INN} (in meV) in bcc Fe obtained with LSDA, corresponding to the vector $\mathbf{R}_{ij} = (\frac{1}{2}, \frac{1}{2}, \frac{1}{2})a$.

	d_{xy}	d_{yz}	d_{xz}	$d_{x^2-y^2}$	$d_{3z^2-r^2}$
d_{xy}	-0.371	-1.500	-1.510	0.000	2.721
d_{yz}	-1.495	-0.370	-1.499	2.031	0.675
d_{xz}	-1.503	-1.503	-0.367	2.031	0.672
$d_{x^2-y^2}$	0.000	2.037	2.025	3.327	0.000
$d_{3z^2-r^2}$	2.710	0.684	0.681	0.000	3.329

Since bcc Fe with partially filled d shell is a typical representative of intermediate correlated materials [101,102], one of the most accurate approaches to describe properties of such a system is the combination of DFT and DMFT, where the electronic structure information is described by DFT while the local correlation effects are handled by DMFT [31–34].

In the DFT + DMFT scheme, we used DFT within the local density approximation (LDA) with non-spin-polarized [95] functional, as implemented in the ELK code [96,97]. Here we used an experimental lattice parameter for bcc Fe of $a_{\text{Fe}} = 2.86 \text{ \AA}$ and a $(20 \times 20 \times 20)$ Monkhorst-Pack \mathbf{k} -point mesh. To perform DMFT calculations, tight-binding Hamiltonian in the basis of maximally localized Wannier functions of spd character on a coarser $(15 \times 15 \times 15)$ \mathbf{k} -point grid was obtained with an ELK to WANNIER90 programming interface [75].

Figure 11 shows the LDA-derived band structure of the nonmagnetic bcc Fe. To parametrize the LDA Hamiltonian, we have constructed the low-energy model in the Wannier functions basis. Using the constructed low-energy model we have performed ferromagnetic LDA + DMFT calculations for bcc Fe.

APPENDIX C: DMFT CALCULATIONS

DMFT equations were solved by AMULET [103] toolbox. The segment version of hybridization expansion continuous-time quantum Monte Carlo (CT-QMC-HYB) solver [104] was used at $T = 300 \text{ K}$, where we set the Coulomb interaction parameter U equal to 2.6 eV while the Hund's J was set as 0.9 eV [105], and appropriate double-counting (DC) correction, based on Friedel sum rule [106], was applied.

We found that the magnetic moment was stabilized at $2.20 \mu_B$ per iron atom. The obtained value agrees well with previous theoretical and experimental studies [24,100] as well

 TABLE IV. Orbital-decomposed J_{INN} (in meV) in bcc Fe obtained with LDA+DMFT, corresponding to the vector $\mathbf{R}_{ij} = (\frac{1}{2}, \frac{1}{2}, \frac{1}{2})a$.

	d_{xy}	d_{yz}	d_{xz}	$d_{x^2-y^2}$	$d_{3z^2-r^2}$
d_{xy}	-0.752	-1.030	-1.031	0.000	2.436
d_{yz}	-1.026	-0.751	-1.027	1.815	0.598
d_{xz}	-1.027	-1.028	-0.753	1.820	0.598
$d_{x^2-y^2}$	0.000	1.817	1.811	3.244	0.000
$d_{3z^2-r^2}$	2.407	0.612	0.612	0.000	3.244

 TABLE V. Orbital-decomposed J_{INN} (in meV) in bcc Fe obtained in [84], corresponding to the vector $\mathbf{R}_{ij} = (\frac{1}{2}, \frac{1}{2}, \frac{1}{2})a$.

	d_{xy}	d_{yz}	d_{xz}	$d_{x^2-y^2}$	$d_{3z^2-r^2}$
d_{xy}	-1.333	-1.659	-1.659	0.000	2.925
d_{yz}	-1.659	-1.333	-1.659	2.190	0.734
d_{xz}	-1.659	-1.659	-1.333	2.190	0.734
$d_{x^2-y^2}$	0.000	2.190	2.190	3.836	0.000
$d_{3z^2-r^2}$	2.925	0.734	0.734	0.000	3.836

as with the results of LSDA calculations, presented earlier in this work.

The main result of the CT-QMC-HYB DMFT solver is local self-energy $\Sigma(i\omega_n)$ on the Matsubara frequencies, i.e., on imaginary energy grid. $\Sigma(i\omega_n)$ can be interpreted as an additional term to the LDA originated non-spin-polarized tight-binding Hamiltonian $H^{\text{LDA}}(\mathbf{k})$ in the Wannier functions basis (LDA + DMFT scheme) and allows to take into account electron-electron correlations effect of an investigated system. Hence, $\Sigma(i\omega_n)$ directly defines intra-atomic spin-splitting and Green's functions. In this sense an additional approximation of analytic continuation to Green's functions and self-energies is required if one would like to use J_{ij} , \mathcal{F} , and $J(\mathbf{q})$ expressions that employ real-energy axis and were previously formulated under Eqs. (10), (16), (19), and (33). The most celebrated approaches for such kind of continuation are Padé approximants [107], maximum entropy method [108], and others [109]. These approaches provide basic insight of studied quantities on real axis, but demonstrate such a drawback as smearing some of the states [109]. The other solution is to give an expression of formulas on the fermionic $i\omega_n$ energy points. Such an approach was previously applied to J_{ij} [89]. Following the idea of Kvashnin *et al.*, we can adopt our formulas to use it on the imaginary energy axis:

$$J_{ij} = \frac{T}{2} \sum_n \text{Re Tr}_L \left[\sum_{\sigma} \Delta_i(i\omega_n) G_{ij}^{\sigma}(i\omega_n) \times \Delta_j(i\omega_n) G_{ji}^{-\sigma}(i\omega_n) \right], \quad (\text{C1})$$

$$\{J_{ij}\}^{\alpha\beta} = \frac{T}{2} \text{Re} \sum_n \{ [\Delta_i(i\omega_n) G_{ij}^{\uparrow}(i\omega_n)]^{\alpha\beta} \times [\Delta_j(i\omega_n) G_{ji}^{\downarrow}(i\omega_n)]^{\beta\alpha} + [\Delta_i(i\omega_n) G_{ij}^{\downarrow}(i\omega_n)]^{\alpha\beta} \times [\Delta_j(i\omega_n) G_{ji}^{\uparrow}(i\omega_n)]^{\beta\alpha} \}, \quad (\text{C2})$$

 TABLE VI. Orbital-decomposed $J_{2\text{NN}}$ (in meV) in bcc Fe obtained with LSDA, corresponding to the vector $\mathbf{R}_{ij} = (0, 0, 1)a$.

	d_{xy}	d_{yz}	d_{xz}	$d_{x^2-y^2}$	$d_{3z^2-r^2}$
d_{xy}	0.555	0.000	0.000	0.000	0.000
d_{yz}	0.000	4.982	0.000	0.000	0.000
d_{xz}	0.000	0.000	4.960	0.000	0.000
$d_{x^2-y^2}$	0.000	0.000	0.000	0.340	0.000
$d_{3z^2-r^2}$	0.000	0.000	0.000	0.000	-1.835

TABLE VII. Orbital-decomposed $J_{2\text{NN}}$ (in meV) in bcc Fe obtained with LDA+DMFT, corresponding to the vector $\mathbf{R}_{ij} = (0, 0, 1)a$.

	d_{xy}	d_{yz}	d_{xz}	$d_{x^2-y^2}$	$d_{3z^2-r^2}$
d_{xy}	-0.064	0.000	0.000	0.000	0.000
d_{yz}	0.000	3.475	0.000	0.000	0.000
d_{xz}	0.000	0.000	3.476	0.000	0.000
$d_{x^2-y^2}$	0.000	0.000	0.000	0.436	0.000
$d_{3z^2-r^2}$	0.000	0.000	0.000	0.000	-2.031

$$\mathcal{F}_i = T \sum_n \text{Re Tr}_L[\Delta_i(i\omega_n)(G_{ii}^\uparrow(i\omega_n) - G_{ii}^\downarrow(i\omega_n))], \quad (\text{C3})$$

$$[J(\mathbf{q})]_{ij} = \frac{TN_k}{2} \sum_n \text{Re Tr}_L \left(\sum_\sigma \sum_{\mathbf{k}} \mathcal{A}_{ij}^\sigma(i\omega_n, \mathbf{k} + \mathbf{q}) \times \mathcal{A}_{ji}^{-\sigma}(i\omega_n, \mathbf{k}) \right), \quad (\text{C4})$$

where T is the temperature. Intra-atomic spin splitting at a given site i then reads like

$$\Delta_i(i\omega_n) = \Sigma_i^\uparrow(i\omega_n) - \Sigma_i^\downarrow(i\omega_n); \quad (\text{C5})$$

the intersite Green's function between sites i and j at a given spin σ reads like

$$\mathcal{G}^\sigma(i\omega_n, \mathbf{k}) = \{i\omega_n - H^{\text{LDA}}(\mathbf{k}) - \Sigma^\sigma(i\omega_n)\}^{-1}, \quad (\text{C6})$$

$$G_{ij}^\sigma(i\omega_n) = \frac{1}{N_k} \sum_{\mathbf{k}} [\mathcal{G}^\sigma(i\omega_n, \mathbf{k})]_{ij} \exp(-i\mathbf{k}\mathbf{T}_{ij}); \quad (\text{C7})$$

and $\mathcal{A}_{ij}^\sigma(i\omega_n, \mathbf{k})$ in (C4) reads like

$$\mathcal{A}_{ij}^\sigma(i\omega_n, \mathbf{k}) = \frac{1}{N_k} \Delta_i(i\omega_n) [\mathcal{G}^\sigma(i\omega_n, \mathbf{k})]_{ij}. \quad (\text{C8})$$

We should note that in the fermionic Matsubara frequencies,

TABLE VIII. Orbital-decomposed $J_{2\text{NN}}$ (in meV) in bcc Fe obtained in [84], corresponding to the vector $\mathbf{R}_{ij} = (0, 0, 1)a$.

	d_{xy}	d_{yz}	d_{xz}	$d_{x^2-y^2}$	$d_{3z^2-r^2}$
d_{xy}	0.217	0.000	0.000	0.000	0.000
d_{yz}	0.000	4.517	0.000	0.000	0.000
d_{xz}	0.000	0.000	4.517	0.000	0.000
$d_{x^2-y^2}$	0.000	0.000	0.000	0.244	0.000
$d_{3z^2-r^2}$	0.000	0.000	0.000	0.000	-1.006

where $\omega_n = 2\pi T(2n + 1)$, the actual number of n depends on the T used in the DMFT calculations.

APPENDIX D: CURIE TEMPERATURE AND THE ORBITAL DECOMPOSITION OF J_{ij} FOR NN AND NEXT-NN IN bcc Fe

As long as \mathcal{J}_i [Eq. (1)] is calculated, it appears straightforward to perform the estimation of the Curie temperature (T_C) in bcc Fe. Indeed, in terms of mean-field approximation (MFA) [110] one can write the simple expression for T_C [38]:

$$k_B T_C = \frac{2}{3} \mathcal{J}_i, \quad (\text{D1})$$

where k_B is the Boltzmann constant. In the case of LSDA it yields 1132 and 870 K using single [Eqs. (9) and (19)] and pairwise [Eq. (17)] infinitesimal spin rotations technique, correspondingly. As expected, both techniques give the same result using LDA + DMFT scheme: $T_C = 895$ K. Although the numerical accordance with the experimental value of 1043 K [111] is generally debatable due to the complicated character of magnetic picture in bcc Fe [89], the thus obtained estimations emphasize the entire consistency of our theoretical approach, supported by the previous studies.

Investigating J_{INN} from Tables III, IV, and V as well as $J_{2\text{NN}}$ from Tables VI, VII, and VIII, we found a good agreement of obtained results with previous studies of decomposed J_{ij} values of bcc Fe.

-
- [1] G. E. Moore, *Electronics* **38**, 114 (1965).
[2] G. E. Moore, *IEEE International Electronic Devices Meeting, 1975* (IEEE, New York, 1975), p. 11.
[3] J. C. Slater and G. F. Koster, *Phys. Rev.* **94**, 1498 (1954).
[4] E. Pavarini (unpublished).
[5] E. Pavarini, E. Koch, F. Anders, and M. Jarrell, *Correlated Electrons: From Models to Materials* (Forschungszentrum Jülich, Verlag, 2012).
[6] E. Pavarini, E. Koch, D. Vollhardt, and A. Lichtenstein, *The LDA+DMFT Approach to Strongly Correlated Materials* (Forschungszentrum Jülich GmbH Institute for Advanced Simulations, Jülich, Germany, 2011).
[7] C. M. Goringe, D. R. Bowler, and E. Hernández, *Rep. Prog. Phys.* **60**, 1447 (1997).
[8] P. YU and M. Cardona, *Fundamentals of Semiconductors: Physics and Materials Properties*, Advanced Texts in Physics, No. 3 (Springer, Berlin, 2005).
[9] A. N. Bogdanov and U. K. Röbler, *Phys. Rev. Lett.* **87**, 037203 (2001).
[10] P. Anderson, *Mater. Res. Bull.* **8**, 153 (1973).
[11] E. Dagotto, *Rev. Mod. Phys.* **66**, 763 (1994).
[12] E. A. Stepanov, A. Huber, E. G. C. P. van Loon, A. I. Lichtenstein, and M. I. Katsnelson, *Phys. Rev. B* **94**, 205110 (2016).
[13] W. Kohn and L. J. Sham, *Phys. Rev.* **140**, A1133 (1965).
[14] G. H. Wannier, *Phys. Rev.* **52**, 191 (1937).
[15] A. I. Lichtenstein, M. I. Katsnelson, and V. A. Gubanov, *J. Phys. F: Met. Phys.* **14**, L125 (1984).
[16] A. Lichtenstein, M. Katsnelson, V. Antropov, and V. Gubanov, *J. Magn. Magn. Mater.* **67**, 65 (1987).
[17] V. Antropov, M. Katsnelson, and A. Lichtenstein, *Phys. B: Condens. Matter* **237-238**, 336 (1997), Proceedings of the Yamada Conference XLV, the International Conference on the Physics of Transition Metals.

- [18] M. I. Katsnelson and A. I. Lichtenstein, *Phys. Rev. B* **61**, 8906 (2000).
- [19] M. Katsnelson and A. Lichtenstein, *J. Phys.: Condens. Matter* **16**, 7439 (2004).
- [20] A. Machintosh and O. Andersen, *Electrons at the Fermi Surface* (Cambridge University Press, Cambridge, 1980), p. 149.
- [21] M. Methfessel and J. Kubler, *J. Phys. F: Met. Phys.* **12**, 141 (1982).
- [22] V. Antropov, B. Harmon, and A. Smirnov, *J. Magn. Magn. Mater.* **200**, 148 (1999).
- [23] P. A. Igoshev, A. V. Efremov, and A. A. Katanin, *Phys. Rev. B* **91**, 195123 (2015).
- [24] Y. O. Kvashnin, R. Cardias, A. Szilva, I. Di Marco, M. I. Katsnelson, A. I. Lichtenstein, L. Nordström, A. B. Klautau, and O. Eriksson, *Phys. Rev. Lett.* **116**, 217202 (2016).
- [25] A. S. Belozerov, A. A. Katanin, and V. I. Anisimov, *Phys. Rev. B* **96**, 075108 (2017).
- [26] I. V. Kashin, S. N. Andreev, and V. V. Mazurenko, *J. Magn. Magn. Mater.* **467**, 58 (2018).
- [27] D. R. Hartree, *Math. Proc. Cambridge Philos. Soc.* **24**, 111 (1928).
- [28] V. Fock, *Z. Phys.* **61**, 126 (1930).
- [29] V. Fock, *Eur. Phys. J. A* **62**, 795 (1930).
- [30] A. Alavi, H. Alloul, R. Eder, M. Foulkes, C. Hess, E. Koch, A. Läuchli, F. Manghi, E. Pavarini, L. Reining, R. Scalettar, G. Sawatzky, J. van den Brink, and D. van der Marel, *Quantum Materials: Experiments and Theory* (Forschungszentrum Jülich GmbH Institute for Advanced Simulations, Jülich, Germany, 2016).
- [31] W. Metzner and D. Vollhardt, *Phys. Rev. Lett.* **62**, 324 (1989).
- [32] A. Georges and G. Kotliar, *Phys. Rev. B* **45**, 6479 (1992).
- [33] A. Georges, G. Kotliar, W. Krauth, and M. J. Rozenberg, *Rev. Mod. Phys.* **68**, 13 (1996).
- [34] G. Kotliar, S. Y. Savrasov, K. Haule, V. S. Oudovenko, O. Parcollet, and C. A. Marianetti, *Rev. Mod. Phys.* **78**, 865 (2006).
- [35] M. A. Ruderman and C. Kittel, *Phys. Rev.* **96**, 99 (1954).
- [36] T. Kasuya, *Prog. Theor. Phys.* **16**, 45 (1956).
- [37] K. Yosida, *Phys. Rev.* **106**, 893 (1957).
- [38] M. Pajda, J. Kudrnovský, I. Turek, V. Drchal, and P. Bruno, *Phys. Rev. B* **64**, 174402 (2001).
- [39] H. Yoon, T. J. Kim, J.-H. Sim, S. W. Jang, T. Ozaki, and M. J. Han, *Phys. Rev. B* **97**, 125132 (2018).
- [40] P. Hohenberg and W. Kohn, *Phys. Rev.* **136**, B864 (1964).
- [41] J. P. Perdew, J. A. Chevary, S. H. Vosko, K. A. Jackson, M. R. Pederson, D. J. Singh, and C. Fiolhais, *Phys. Rev. B* **46**, 6671 (1992).
- [42] V. I. Anisimov, J. Zaanen, and O. K. Andersen, *Phys. Rev. B* **44**, 943 (1991).
- [43] N. Marzari and D. Vanderbilt, *Phys. Rev. B* **56**, 12847 (1997).
- [44] N. Marzari, A. A. Mostofi, J. R. Yates, I. Souza, and D. Vanderbilt, *Rev. Mod. Phys.* **84**, 1419 (2012).
- [45] H. J. Monkhorst and J. D. Pack, *Phys. Rev. B* **13**, 5188 (1976).
- [46] A. Lichtenstein, *Magnetism: From Stoner to Hubbard* (Forschungszentrum Jülich GmbH Institute for Advanced Simulations, Jülich, Germany, 2013).
- [47] I. Kashin, V. Mazurenko, M. Katsnelson, and A. Rudenko, *2D Mater.* **7**, 025036 (2020).
- [48] V. V. Mazurenko, Y. O. Kvashnin, A. I. Lichtenstein, and M. I. Katsnelson, *J. Exp. Theor. Phys.* **132**, 506 (2021).
- [49] M. I. Katsnelson, Y. O. Kvashnin, V. V. Mazurenko, and A. I. Lichtenstein, *Phys. Rev. B* **82**, 100403(R) (2010).
- [50] V. E. Dmitrienko, E. N. Ovchinnikova, S. P. Collins, G. Nisbet, G. Beutier, Y. O. Kvashnin, V. V. Mazurenko, A. I. Lichtenstein, and M. I. Katsnelson, *Nat. Phys.* **10**, 202 (2014).
- [51] S.-T. Pi, S. Y. Savrasov, and W. E. Pickett, *Phys. Rev. Lett.* **122**, 057201 (2019).
- [52] X. Wan, T. A. Maier, and S. Y. Savrasov, *Phys. Rev. B* **79**, 155114 (2009).
- [53] M. J. Han, Q. Yin, W. E. Pickett, and S. Y. Savrasov, *Phys. Rev. Lett.* **102**, 107003 (2009).
- [54] X. He, N. Helbig, M. J. Verstraete, and E. Bousquet, *Comput. Phys. Commun.* **264**, 107938 (2021).
- [55] I. V. Solovyev, I. V. Kashin, and V. V. Mazurenko, *Phys. Rev. B* **92**, 144407 (2015).
- [56] H. Okumura, K. Sato, and T. Kotani, *Phys. Rev. B* **100**, 054419 (2019).
- [57] T. Fukazawa, H. Akai, Y. Harashima, and T. Miyake, *J. Magn. Magn. Mater.* **469**, 296 (2019).
- [58] I. V. Solovyev and K. Terakura, *Phys. Rev. Lett.* **82**, 2959 (1999).
- [59] I. V. Solovyev and K. Terakura, *Phys. Rev. B* **58**, 15496 (1998).
- [60] M. Modarresi, A. Mogulkoc, Y. Mogulkoc, and A. N. Rudenko, *Phys. Rev. Appl.* **11**, 064015 (2019).
- [61] V. V. Mazurenko, A. O. Shorikov, A. V. Lukoyanov, K. Kharlov, E. Gorelov, A. I. Lichtenstein, and V. I. Anisimov, *Phys. Rev. B* **81**, 125131 (2010).
- [62] S. L. Dudarev, G. A. Botton, S. Y. Savrasov, C. J. Humphreys, and A. P. Sutton, *Phys. Rev. B* **57**, 1505 (1998).
- [63] R. Logemann, A. N. Rudenko, M. I. Katsnelson, and A. Kirilyuk, *J. Phys.: Condens. Matter* **29**, 335801 (2017).
- [64] I. Solovyev, N. Hamada, and K. Terakura, *Phys. Rev. Lett.* **76**, 4825 (1996).
- [65] I. Solovyev, N. Hamada, and K. Terakura, *Phys. Rev. B* **53**, 7158 (1996).
- [66] P. Werner and A. J. Millis, *Phys. Rev. Lett.* **99**, 126405 (2007).
- [67] C. S. Wang, B. M. Klein, and H. Krakauer, *Phys. Rev. Lett.* **54**, 1852 (1985).
- [68] K. Terakura, A. R. Williams, T. Oguchi, and J. Kübler, *Phys. Rev. Lett.* **52**, 1830 (1984).
- [69] K. Terakura, T. Oguchi, A. R. Williams, and J. Kübler, *Phys. Rev. B* **30**, 4734 (1984).
- [70] A. A. Dyachenko, A. O. Shorikov, A. V. Lukoyanov, and V. I. Anisimov, *JETP Lett.* **96**, 56 (2012).
- [71] A. Droghetti, C. D. Pemmaraju, and S. Sanvito, *Phys. Rev. B* **78**, 140404(R) (2008).
- [72] J. M. Rondinelli, N. M. Caffrey, S. Sanvito, and N. A. Spaldin, *Phys. Rev. B* **78**, 155107 (2008).
- [73] S. K. Panda, P. Thunström, I. D. Marco, J. Schött, A. Delin, I. Dasgupta, O. Eriksson, and D. D. Sarma, *New J. Phys.* **16**, 093049 (2014).
- [74] A. O. Shorikov, S. V. Streltsov, and M. A. Korotin, *JETP Lett.* **102**, 616 (2015).
- [75] A. Gerasimov, L. Nordström, S. Khmelevskyi, V. Mazurenko, and Y. Kvashnin, *J. Phys.: Condens. Matter* **33**, 165801 (2021).
- [76] A. S. Belozerov and V. I. Anisimov, *J. Phys.: Condens. Matter* **28**, 345601 (2016).
- [77] S. Y. Savrasov and G. Kotliar, *Phys. Rev. Lett.* **90**, 056401 (2003).

- [78] S. N. Iskakov, V. V. Mazurenko, M. V. Valentyuk, and A. I. Lichtenstein, *Phys. Rev. B* **92**, 245135 (2015).
- [79] V. V. Mazurenko, S. N. Iskakov, A. N. Rudenko, I. V. Kashin, O. M. Sotnikov, M. V. Valentyuk, and A. I. Lichtenstein, *Phys. Rev. B* **88**, 085112 (2013).
- [80] K. Haule, *Phys. Rev. Lett.* **115**, 196403 (2015).
- [81] E. A. Stepanov, S. Brener, F. Krien, M. Harland, A. I. Lichtenstein, and M. I. Katsnelson, *Phys. Rev. Lett.* **121**, 037204 (2018).
- [82] E. A. Stepanov, A. Huber, A. I. Lichtenstein, and M. I. Katsnelson, *Phys. Rev. B* **99**, 115124 (2019).
- [83] E. A. Stepanov, S. Brener, V. Harkov, M. I. Katsnelson, and A. I. Lichtenstein, *Phys. Rev. B* **105**, 155151 (2022).
- [84] R. Cardias, A. Szilva, A. Bergman, I. Marco, M. Katsnelson, A. Lichtenstein, L. Nordström, A. Klautau, O. Eriksson, and Y. Kvashnin, *Sci. Rep.* **7**, 4058 (2017).
- [85] H. Wang, P.-W. Ma, and C. H. Woo, *Phys. Rev. B* **82**, 144304 (2010).
- [86] A. Jacobsson, B. Sanyal, M. Ležaić, and S. Blügel, *Phys. Rev. B* **88**, 134427 (2013).
- [87] A. Jacobsson, G. Johansson, O. I. Gorbatov, M. Ležaić, B. Sanyal, S. Blügel, and C. Etz, Parameterisation of non-collinear energy landscapes in itinerant magnets, [arXiv:1702.00599](https://arxiv.org/abs/1702.00599).
- [88] I. Turek, J. Kudrnovský, V. Drchal, and P. Bruno, *Philos. Mag.* **86**, 1713 (2006).
- [89] Y. O. Kvashnin, O. Grånäs, I. Di Marco, M. I. Katsnelson, A. I. Lichtenstein, and O. Eriksson, *Phys. Rev. B* **91**, 125133 (2015).
- [90] T. Tanaka and Y. Gohda, *npj Comput. Mater.* **6**, 184 (2020).
- [91] A. Szilva, D. Thonig, P. F. Bessarab, Y. O. Kvashnin, D. C. M. Rodrigues, R. Cardias, M. Pereiro, L. Nordström, A. Bergman, A. B. Klautau, and O. Eriksson, *Phys. Rev. B* **96**, 144413 (2017).
- [92] E. Stade, *Fourier Analysis*, Pure and Applied Mathematics: A Wiley Series of Texts, Monographs and Tracts (Wiley, Hoboken, NJ, 2011).
- [93] S. Tiwari, M. L. Van de Put, B. Sorée, and W. G. Vandenberghe, *Phys. Rev. B* **103**, 014432 (2021).
- [94] S. Tiwari, M. L. Van de Put, B. Sorée, and W. G. Vandenberghe, *npj 2D Mater. Appl.* **5**, 54 (2021).
- [95] J. P. Perdew and Y. Wang, *Phys. Rev. B* **45**, 13244 (1992).
- [96] ELK, an all-electron full-potential linearized augmented plane wave plus local orbitals *FP-LAPW+lo* code, elk.sourceforge.net.
- [97] D. Singh, *Planewaves, Pseudopotentials and the LAPW Method* (Springer, New York, 2013).
- [98] A. A. Mostofi, J. R. Yates, Y.-S. Lee, I. Souza, D. Vanderbilt, and N. Marzari, *Comput. Phys. Commun.* **178**, 685 (2008).
- [99] A. A. Mostofi, J. R. Yates, G. Pizzi, Y.-S. Lee, I. Souza, D. Vanderbilt, and N. Marzari, *Comput. Phys. Commun.* **185**, 2309 (2014).
- [100] I. M. L. Billas, J. A. Becker, A. Châtelain, and W. A. de Heer, *Phys. Rev. Lett.* **71**, 4067 (1993).
- [101] V. Anisimov and Y. Izyumov, *Electronic Structure of Strongly Correlated Materials* (Springer, Berlin, 2010), Vol. 163.
- [102] M. I. Katsnelson and A. I. Lichtenstein, *J. Phys.: Condens. Matter* **11**, 1037 (1999).
- [103] AMULET, amulet-code.org.
- [104] E. Gull, A. J. Millis, A. I. Lichtenstein, A. N. Rubtsov, M. Troyer, and P. Werner, *Rev. Mod. Phys.* **83**, 349 (2011).
- [105] L. I. Yin, T. Tsang, and I. Adler, *Phys. Rev. B* **15**, 2974 (1977).
- [106] B. Amadon, F. Lechermann, A. Georges, F. Jollet, T. O. Wehling, and A. I. Lichtenstein, *Phys. Rev. B* **77**, 205112 (2008).
- [107] H. J. Vidberg and J. W. Serene, *J. Low Temp. Phys.* **29**, 179 (1977).
- [108] A. W. Sandvik, *Phys. Rev. B* **57**, 10287 (1998).
- [109] J. Schött, I. L. M. Locht, E. Lundin, O. Grånäs, O. Eriksson, and I. Di Marco, *Phys. Rev. B* **93**, 075104 (2016).
- [110] E. Şaşıoğlu, L. M. Sandratskii, and P. Bruno, *Phys. Rev. B* **70**, 024427 (2004).
- [111] Y. Touloukian, R. Kirby, R. Taylor, and P. Desai, *Thermal Expansion: Thermophysical Properties of Matter* (Plenum, New York, 1975), Vol. 12.